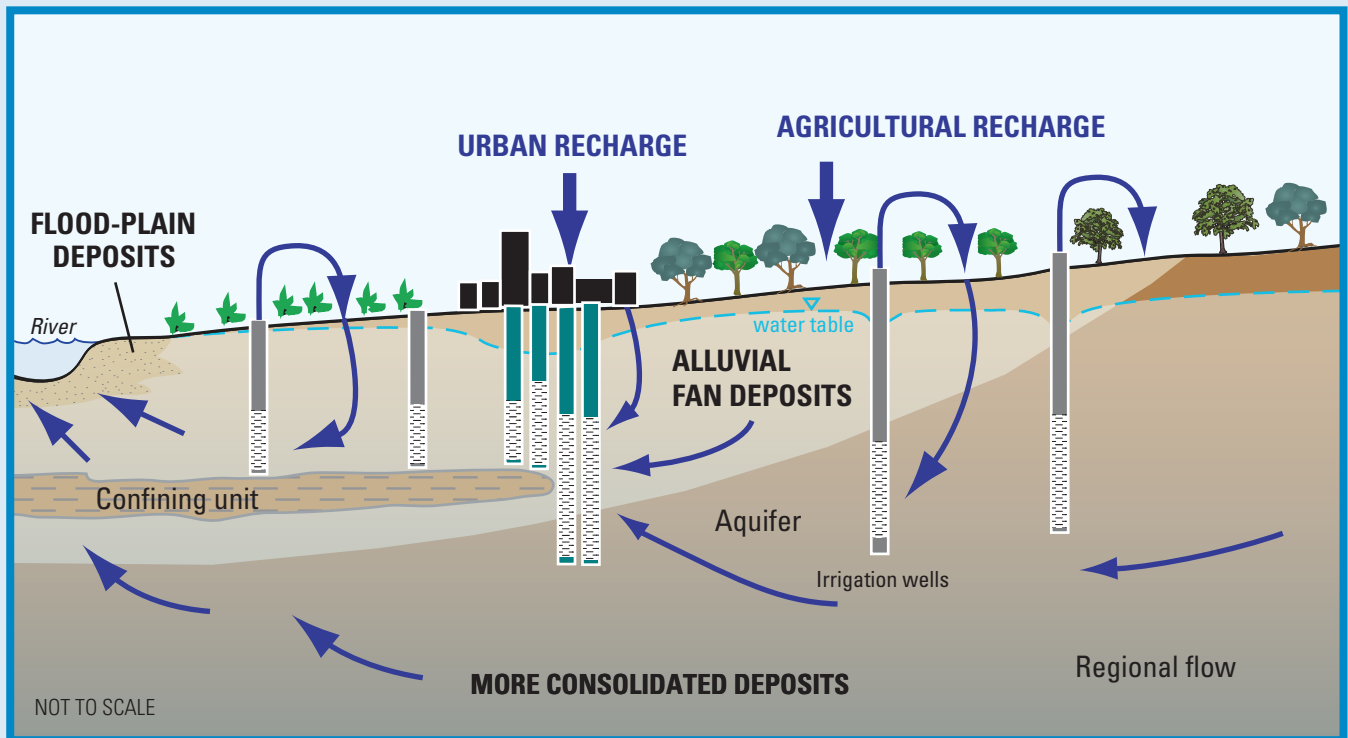


**National Water-Quality Assessment Program  
Transport of Anthropogenic and Natural  
Contaminants (TANC) to Public-Supply Wells**

# **Simulations of Ground-Water Flow and Particle Pathline Analysis in the Zone of Contribution of a Public-Supply Well in Modesto, Eastern San Joaquin Valley, California**



Scientific Investigations Report 2008–5035



# **Simulations of Ground-Water Flow and Particle Pathline Analysis in the Zone of Contribution of a Public-Supply Well in Modesto, Eastern San Joaquin Valley, California**

By Karen R. Burow, Bryant C. Jurgens, Leon J. Kauffman, Steven P. Phillips, Barbara A. Dalgish, and Jennifer L. Shelton

National Water-Quality Assessment Program  
Transport of Anthropogenic and Natural Contaminants (TANC)  
to Public-Supply Wells

Scientific Investigations Report 2008–5035

**U.S. Department of the Interior**  
**U.S. Geological Survey**

**U.S. Department of the Interior**  
DIRK KEMPTHORNE, Secretary

**U.S. Geological Survey**  
Mark D. Myers, Director

U.S. Geological Survey, Reston, Virginia: 2008

For product and ordering information:

World Wide Web: <http://www.usgs.gov/pubprod>

Telephone: 1-888-ASK-USGS

For more information on the USGS--the Federal source for science about the Earth, its natural and living resources, natural hazards, and the environment:

World Wide Web: <http://www.usgs.gov>

Telephone: 1-888-ASK-USGS

Any use of trade, product, or firm names is for descriptive purposes only and does not imply endorsement by the U.S. Government.

Although this report is in the public domain, permission must be secured from the individual copyright owners to reproduce any copyrighted materials contained within this report.

Suggested reference:

Burow, K.R., Jurgens, B.C., Kauffman, L.J. Phillips, S.P., Dalgish, B.A., and Shelton, J.L., 2008, Simulations of ground-water flow and particle pathline analysis in the zone of contribution of a public-supply well in Modesto, eastern San Joaquin Valley, California: U.S. Geological Survey Scientific Investigations Report 2008-5035, 41 p. Available at <http://pubs.usgs.gov/sir/2008/5035>

## Foreword

The U.S. Geological Survey (USGS) is committed to providing the Nation with credible scientific information that helps to enhance and protect the overall quality of life and that facilitates effective management of water, biological, energy, and mineral resources (<http://www.usgs.gov/>). Information on the Nation's water resources is critical to ensuring long-term availability of water that is safe for drinking and recreation and is suitable for industry, irrigation, and fish and wildlife. Population growth and increasing demands for water make the availability of that water, now measured in terms of quantity and quality, even more essential to the long-term sustainability of our communities and ecosystems.

The USGS implemented the National Water-Quality Assessment (NAWQA) Program in 1991 to support national, regional, State, and local information needs and decisions related to water-quality management and policy (<http://water.usgs.gov/nawqa>). The NAWQA Program is designed to answer: What is the condition of our Nation's streams and ground water? How are conditions changing over time? How do natural features and human activities affect the quality of streams and ground water, and where are those effects most pronounced? By combining information on water chemistry, physical characteristics, stream habitat, and aquatic life, the NAWQA Program aims to provide science-based insights for current and emerging water issues and priorities. From 1991–2001, the NAWQA Program completed interdisciplinary assessments and established a baseline understanding of water-quality conditions in 51 of the Nation's river basins and aquifers, referred to as Study Units (<http://water.usgs.gov/nawqa/studyu.html>).

Multiple national and regional assessments are ongoing in the second decade (2001–2012) of the NAWQA Program as 42 of the 51 Study Units are reassessed. These assessments extend the findings in the Study Units by determining status and trends at sites that have been consistently monitored for more than a decade, and filling critical gaps in characterizing the quality of surface water and ground water. For example, increased emphasis has been placed on assessing the quality of source water and finished water associated with many of the Nation's largest community water systems. During the second decade, NAWQA is addressing five national priority topics that build an understanding of how natural features and human activities affect water quality, and establish links between sources of contaminants, the transport of those contaminants through the hydrologic system, and the potential effects of contaminants on humans and aquatic ecosystems. Included are topics on the fate of agricultural chemicals, effects of urbanization on stream ecosystems, bioaccumulation of mercury in stream ecosystems, effects of nutrient enrichment on aquatic ecosystems, and transport of contaminants to public-supply wells. These topical studies are conducted in those Study Units most affected by these issues; they comprise a set of multi-Study-Unit designs for systematic national assessment. In addition, national syntheses of information on pesticides, volatile organic compounds (VOCs), nutrients, selected trace elements, and aquatic ecology are continuing.

The USGS aims to disseminate credible, timely, and relevant science information to address practical and effective water-resource management and strategies that protect and restore water quality. We hope this NAWQA publication will provide you with insights and information to meet your needs, and will foster increased citizen awareness and involvement in the protection and restoration of our Nation's waters.

The USGS recognizes that a national assessment by a single program cannot address all water-resource issues of interest. External coordination at all levels is critical for cost-effective management, regulation, and conservation of our Nation's water resources. The NAWQA Program, therefore, depends on advice and information from other agencies—Federal, State, regional, interstate, Tribal, and local—as well as nongovernmental organizations, industry, academia, and other stakeholder groups. Your assistance and suggestions are greatly appreciated.

Matthew C. Larsen  
Acting Associate Director for Water

This page intentionally left blank.

# Contents

|  |    |
|--|----|
| Abstract .....   | 1  |
| Introduction.....  | 2  |
| Background on Public-Supply-Well Vulnerability .....   | 2  |
| Purpose and Scope .....  | 4  |
| Description of Study Area .....  | 4  |
| Hydrogeologic Setting .....  | 4  |
| Land and Water Use.....  | 5  |
| Ground-Water Flow System.....  | 5  |
| Ground-Water Quality in Modesto Public-Supply Wells.....   | 6  |
| Public-Supply Well Selection .....   | 6  |
| Ground-Water Flow Model.....   | 6  |
| Regional Ground-Water Flow Model .....   | 8  |
| Local Ground-Water Flow Model .....  | 8  |
| Model Geometry and Discretization .....  | 8  |
| Boundary Conditions, Model Stresses, and Initial Conditions .....  | 9  |
| Aquifer Hydraulic Conductivity.....  | 11 |
| Hydrofacies Classification .....   | 11 |
| Spatial Correlation Model of Hydrofacies .....   | 12 |
| Ground-Water Flow Model Calibration .....  | 12 |
| Sensitivity Analysis.....  | 17 |
| Ground-Water Flow Model Results .....  | 17 |
| Simulated Water Levels and Flows.....  | 17 |
| Simulated Budget .....   | 17 |
| Simulation of Advective Transport by Particle Tracking .....   | 17 |
| Methods and Model Parameters .....   | 21 |
| Particle Tracking Results and Comparison to Age Tracer Concentrations .....  | 22 |
| Comparison between Land Use in the Contributing Recharge Area (CRA) and<br>Occurrence of Selected Constituents ..... | 25 |
| Processes Affecting Nitrate and Uranium Concentrations in the Aquifer and the<br>Public-Supply Well .....            | 29 |
| Long-Term Concentrations of Nitrate and Uranium in the Public-Supply Well.....                                       | 33 |
| Model Uncertainties and Limitations .....  | 36 |
| Summary and Conclusions.....   | 36 |
| Acknowledgments.....   | 37 |
| References Cited.....  | 38 |

## Figures

|            |  |    |
|------------|--|----|
| Figure 1.  | Map showing study area near Modesto in the eastern San Joaquin Valley, California .....  | 3  |
| Figure 2.  | Map showing extent of local ground-water flow model nested within regional model of an area near Modesto, eastern San Joaquin Valley, California .....   | 7  |
| Figure 3.  | Map showing boundary conditions and distribution of recharge specified in the local ground-water flow model near Modesto, eastern San Joaquin Valley, California .....   | 10 |
| Figure 4.  | Graphs showing hydrofacies distribution used in the ground-water flow model near Modesto, eastern San Joaquin Valley, California .....   | 13 |
| Figure 5.  | Graphs showing (A) simulated and measured water level and (B) weighted residuals for the calibrated local ground-water flow model near Modesto, eastern San Joaquin Valley, California .....   | 16 |
| Figure 6.  | Graph showing comparison between boundary flows in the regional model and boundary flows in the calibrated local ground-water flow model near Modesto, eastern San Joaquin Valley, California .....  | 17 |
| Figure 7.  | Graphs showing sensitivity of model parameters with respect to (A) sum of squared residuals of simulated and measured water levels, (B) net flow through upgradient (east) boundary, and (C) net flow through downgradient (west) boundary ..... | 18 |
| Figure 8.  | Map showing simulated water table elevation in local ground-water flow model near Modesto, eastern San Joaquin Valley, California .....  | 19 |
| Figure 9.  | Map showing simulated water level in model layer 150 in local ground-water flow model near Modesto, eastern San Joaquin Valley, California .....   | 20 |
| Figure 10. | Graph showing simulated water level along vertical transect A-A' in local ground-water flow model near Modesto, eastern San Joaquin Valley, California .....   | 21 |
| Figure 11. | Map showing contributing recharge area and particle travel times to public-supply well near Modesto, eastern San Joaquin Valley, California .....  | 23 |
| Figure 12. | Graph showing simulated flow-weighted age of particles reaching the public-supply well near Modesto, eastern San Joaquin Valley, California .....  | 24 |
| Figure 13. | Graph showing simulated age and interpreted ground-water age from age-dating tracers, as compared with depth below water table in monitoring wells and the public-supply well near Modesto, eastern San Joaquin Valley, California .....         | 25 |
| Figure 14. | Graph showing concentrations of tritium ( $^3\text{H}$ ) and sulfur hexafluoride ( $\text{SF}_6$ ) in recharge .....   | 26 |
| Figure 15. | Graphs showing simulated and measured concentrations of (A) sulfur hexafluoride ( $\text{SF}_6$ ) and (B) tritium ( $^3\text{H}$ ) in monitoring wells and the public-supply well near Modesto, eastern San Joaquin Valley, California .....     | 27 |
| Figure 16. | Graph showing simulated and measured tritium ( $^3\text{H}$ ) concentrations with depth in monitoring wells and the public-supply well near Modesto, eastern San Joaquin Valley, California .....  | 27 |
| Figure 17. | Graph showing estimated concentrations of nitrate in recharge from nitrogen fertilizer applications over time and measured nitrate concentrations in monitoring wells .....  | 31 |
| Figure 18. | Graph showing simulated and measured concentrations of nitrate in monitoring wells and the public-supply well near Modesto, eastern San Joaquin Valley, California .....   | 32 |



|   |    |
|---|----|
| Figure 19. Graph showing alkalinity and uranium concentrations in monitoring wells at different depths and in the public-supply well near Modesto, eastern San Joaquin Valley, California ..... | 33 |
| Figure 20. Graph showing simulated and measured alkalinity in monitoring wells and the public-supply well near Modesto, eastern San Joaquin Valley, California .....                            | 34 |
| Figure 21. Graph showing simulated long-term concentrations of nitrate in the public-supply well near Modesto, eastern San Joaquin Valley, California .....                                     | 35 |
| Figure 22. Graph showing simulated long-term alkalinity and inferred uranium concentrations in the public-supply well near Modesto, eastern San Joaquin Valley, California .....                | 35 |

## Tables

|  |    |
|--|----|
| Table 1. Well depths and pumping rates assigned to wells in the local ground-water flow model near Modesto, eastern San Joaquin Valley, California .....   | 11 |
| Table 2. Embedded transition probability matrices and mean hydrofacies lengths in the geologic model near Modesto, eastern San Joaquin Valley, California .....  | 12 |
| Table 3. Hydraulic conductivity of hydrofacies used in the local ground-water flow model near Modesto, eastern San Joaquin Valley, California .....  | 15 |
| Table 4. Volumetric budget of local ground-water flow model near Modesto, eastern San Joaquin Valley, California .....   | 21 |
| Table 5. Summary statistics for the simulated contributing recharge area and the zone of contribution of the public-supply well near Modesto, eastern San Joaquin Valley, California .....   | 24 |
| Table 6. Well characteristics and simulated and interpreted ground-water ages from age-dating tracers in monitoring wells sampled in 2003–2005 near Modesto, eastern San Joaquin Valley, California .....  | 26 |
| Table 7. Nitrate concentrations, volatile organic compound and pesticide occurrence, and relation to land use in the contributing recharge areas of the public-supply well and monitoring wells in Modesto, eastern San Joaquin Valley, California ... | 28 |
| Table 8. Nitrate, alkalinity and uranium concentrations from monitoring wells and the public-supply well sampled in 2003–2005 near Modesto, eastern San Joaquin Valley, California .....   | 30 |

## Conversion Factors, Spatial Datums, Abbreviations, and Acronyms

### SI to Inch/Pound

| Multiply                                     | By        | To obtain                               |
|--|-----------|---|
| <b>Length</b>                                |           |   |
| millimeter (mm)                              | 0.03937   | inch (in.)                              |
| meter (m)                                    | 3.281     | foot (ft)                               |
| kilometer (km)                               | 0.6214    | mile (mi)                               |
| <b>Area</b>                                  |           |   |
| square meter (m <sup>2</sup> )               | 0.0002471 | acre                                    |
| square kilometer (km <sup>2</sup> )          | 247.1     | acre                                    |
| <b>Flow rate</b>                             |           |   |
| cubic meter per day (m <sup>3</sup> /d)      | 0.000264  | million gallons per day (Mgal/d)        |
| cubic meter per day (m <sup>3</sup> /d)      | 35.31     | cubic foot per day (ft <sup>3</sup> /d) |
| cubic meter per minute (m <sup>3</sup> /min) | 264.2     | gallon per minute (gal/min)             |
| meter per day (m/d)                          | 3.281     | foot per day (ft/d)                     |
| meter per year (m/yr)                        | 3.281     | foot per year (ft/yr)                   |

## Spatial Datums

Vertical coordinate information is referenced to the North American Vertical Datum of 1988 (NAVD 88).

Elevation, as used in this report, refers to distance above the vertical datum.

Horizontal coordinate information is referenced to the North American Datum of 1983 (NAD 83).

Concentrations of chemical constituents in water are given either in milligrams per liter (mg/L) or micrograms per liter (µg/L).

## Abbreviations and Acronyms

|                   |   |
|-------------------|---|
| CRA,              | contributing recharge area                          |
| <sup>3</sup> H,   | tritium   |
| MCL,              | maximum contaminant level                           |
| NAWQA,            | National Water-Quality Assessment Program           |
| PSW               | public-supply well                                  |
| SF <sub>6</sub> , | sulfur hexafluoride                                 |
| TANC,             | transport of anthropogenic and natural contaminants |
| USGS,             | U.S Geological Survey                               |
| VOC,              | volatile organic compounds                          |
| ZOC,              | zone of contribution                                |

# Simulations of Ground-Water Flow and Particle Pathline Analysis in the Zone of Contribution of a Public-Supply Well in Modesto, Eastern San Joaquin Valley, California

By Karen R. Burow, Bryant C. Jurgens, Leon J. Kauffman, Steven P. Phillips, Barbara A. Dalgish, and Jennifer L. Shelton

## Abstract

Shallow ground water in the eastern San Joaquin Valley is affected by high nitrate and uranium concentrations and frequent detections of pesticides and volatile organic compounds (VOC), as a result of ground-water development and intensive agricultural and urban land use. A single public-supply well was selected for intensive study to evaluate the dominant processes affecting the vulnerability of public-supply wells in the Modesto area. A network of 23 monitoring wells was installed, and water and sediment samples were collected within the approximate zone of contribution of the public-supply well, to support a detailed analysis of physical and chemical conditions and processes affecting the water chemistry in the well. A three-dimensional, steady-state local ground-water-flow and transport model was developed to evaluate the age of ground water reaching the well and to evaluate the vulnerability of the well to nonpoint source input of nitrate and uranium.

Particle tracking was used to compute pathlines and advective travel times in the ground-water flow model. The simulated ages of particles reaching the public-supply well ranged from 9 to 30,000 years, with a median of 54 years. The age of the ground water contributed to the public-supply well increased with depth below the water table. Measured nitrate concentrations, derived primarily from agricultural fertilizer, were highest (17 milligrams per liter) in shallow ground water and decreased with depth to background concentrations of less than 2 milligrams per liter in the deepest wells. Because the movement of water is predominantly downward as a result of ground-water development, and because geochemical conditions are generally oxic, high nitrate concentrations in shallow ground water are expected to continue moving downward without significant attenuation. Simulated long-

term nitrate concentrations indicate that concentrations have peaked and will decrease in the public-supply well during the next 100 years because of the low nitrate concentrations in recharge beneath the urban area and the increasing proportion of urban-derived ground water reaching the well. The apparent lag time between peak input concentrations and peak concentrations in the well is about 20 to 30 years.

Measured uranium concentrations were also highest (45 micrograms per liter) in shallow ground water, and decreased with depth to background concentrations of about 0.5 microgram per liter. Naturally-occurring uranium adsorbed to aquifer sediments is mobilized by oxygen-rich, high-alkalinity water. Alkalinity increased in shallow ground water in response to agricultural development. As ground-water pumping increased in the 1940s and 1950s, this high-alkalinity water moved downward through the ground-water flow system, mobilizing the uranium adsorbed to aquifer sediments. Ground water with high alkalinity and high uranium concentrations is expected to continue to move deeper in the system, resulting in increased uranium concentrations with depth in ground water. Because alkalinity (and correspondingly uranium) concentrations were high in shallow ground water beneath both the urban and the agricultural land, long-term uranium concentrations in the public-supply well are expected to increase as the proportion of uranium-affected water contributed to the well increases. Assuming that the alkalinity near the water table remains the same, the simulation of long-term alkalinity in the public-supply well indicates that uranium concentrations in the public-supply well will likely approach the maximum contaminant level; however, the time to reach this level is more than 100 years because of the significant proportion of old, unaffected water at depth that is contributed to the public-supply well.

## Introduction

In 2000, ground water provided 37 percent of the public drinking-water supplies used by 242 million people nationwide (Hutson and others, 2004). Withdrawals of ground water for public supply has increased five fold over the last 50 years, causing increased concern about the quality of water pumped by public-supply wells. California withdraws more ground water for public supply than any other state in the nation, serving more than 30 million people and accounting for 18 percent of the total ground-water withdrawals for public supply in 2000 (Hutson and others, 2004).

The use of ground water for public supply is threatened by compounds that have been introduced by human activities. Volatile organic compounds (VOC) were detected in 90 of 98 aquifer studies completed across the nation; California led most other states in detection frequencies (Zogorski and others, 2006). Nationwide, pesticides were detected in more than 50 percent of wells in shallow ground water (Gilliom and others, 2006). Nitrate was detected in 71 percent of wells in shallow ground water, and concentrations were above the maximum contaminant level (MCL) of 10 mg/L, as N (U.S. Environmental Protection Agency, 2006) in at least one well out of 20 to 30 wells in nearly one-half of the 33 major aquifers studied (Nolan and Stoner, 2000).

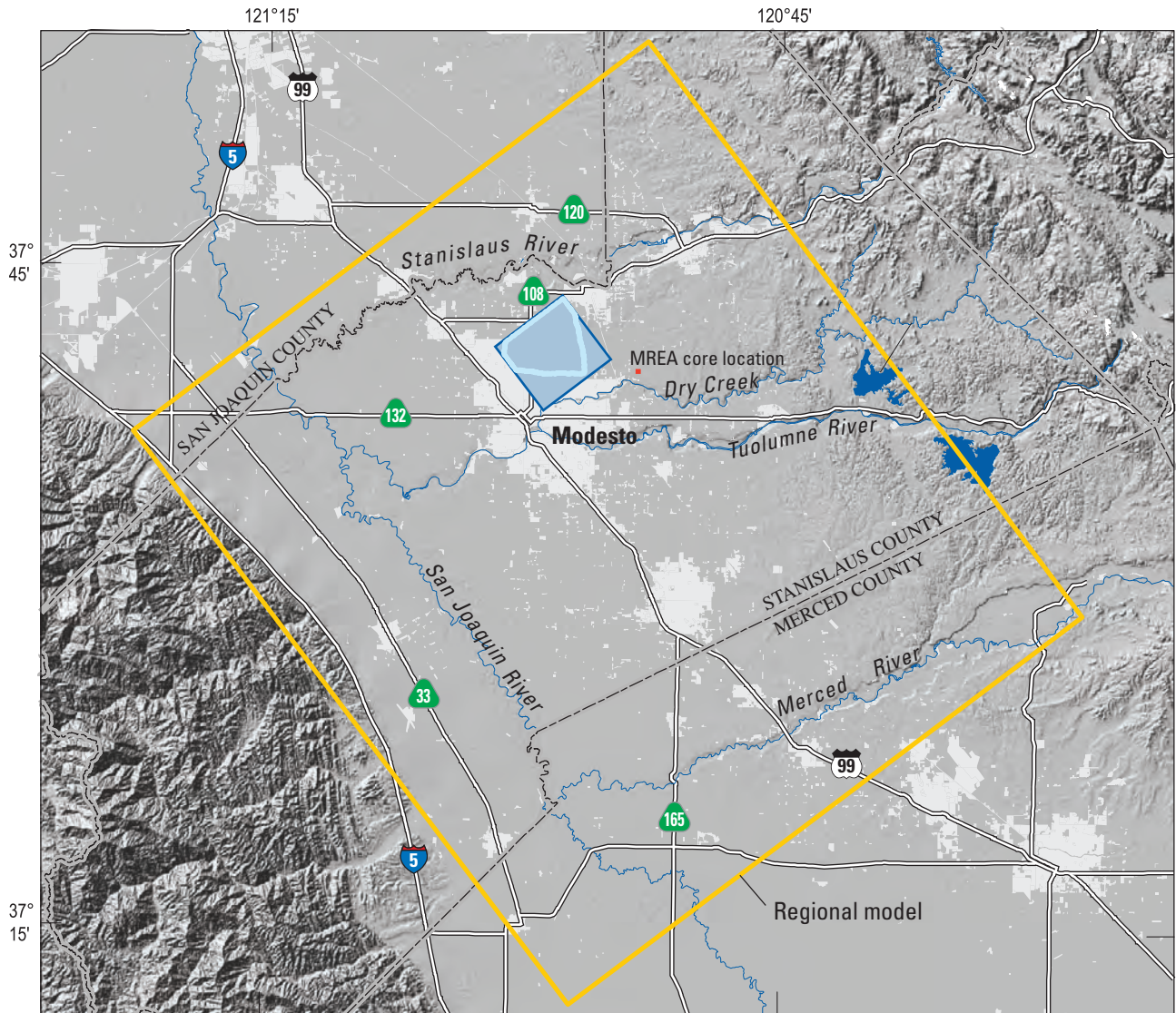
In the eastern San Joaquin Valley, California ([fig. 1](#)), agricultural withdrawals are the dominant water use; however, increased reliance on ground-water withdrawals for public-supply will likely result from the rapid population growth and periods of drought. In shallow ground water, pesticides were detected in 69 percent of domestic wells, and nitrate concentrations were above the MCL in 24 percent of domestic wells sampled during 1993–95 (Dubrovsky and others, 1998). Low concentrations of VOCs were detected in more than 70 percent of public-supply wells sampled in Fresno and more than 90 percent of wells in Modesto in 2001–02 (Wright and others, 2004). Concentrations of nitrate and detections of pesticides in the deep part of the aquifer system, where public-supply wells typically are screened, will likely increase as the proportion of young water contributed to these wells increases (Burow and others, 2007). Sustainability of ground-water quality for present and future public supply requires monitoring and understanding of the mechanisms controlling the vulnerability of public-supply wells to contamination.

## Background on Public-Supply-Well Vulnerability

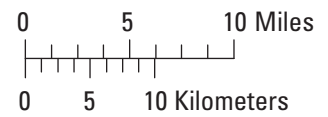
Aquifer and public-supply-well susceptibility to contamination is a function of the intrinsic conditions of an aquifer, such as depth to water, flow-system confinement, recharge rate, hydraulic conductivity, porosity, pumping rate, and geochemical conditions (Focazio and others, 2002). Public-supply-well vulnerability is determined by assessing aquifer susceptibility and potential contaminant sources overlying or within the area contributing recharge to the well (Franke and others, 1998; Focazio and others, 2002). In this report, the word “contaminant” is defined as any natural or anthropogenic chemical or physical property of the ground-water resource in question that could threaten human health, interfere with water-treatment practices (Focazio and others, 2002), or cause other problems.

Several methods have been used to protect public water supplies by determining the susceptibility or vulnerability of an aquifer to contamination. Process-based methods attempt to predict contaminant transport paths at either regional or site-specific scales using model simulation techniques (National Research Council, 1993). The strength of process-based approaches is the ability to differentiate the effects of the underlying processes controlling transport, such as geochemical transformations, contaminant source loading, ground-water velocity, and diffusion and dispersion processes. In process-based studies of public-supply-well vulnerability, the land use above the contributing recharge area of a public-supply well, the travel times of ground water flowing to the well, and aquifer stresses such as well pumping rates are important factors affecting the sources and fate of contaminants reaching the wells (Reilly and Gibs, 1993; Reilly and Pollock, 1995; Johnson and others, 2000; Kauffman and others, 2001; Brown and others, 2002). However, lack of data, and the averaging of variables over scales that fail to capture the inherent physical and chemical heterogeneity of the system impair the ability of models to quantify contributing areas to wells (Reilly and Pollock, 1993; Barlow, 1997; Focazio and others, 2002; Harrar and others, 2003). Additionally, many models do not adequately represent alternative pathways for contaminants to reach wells, such as short-circuits through wellbores or unmapped layers of high hydraulic conductivity (Franke and others, 1998; Cole and Silliman, 2000). Additionally, natural contaminants such as trace elements, radionuclides, or salinity are rarely considered because of the difficulty in mapping the source areas and the subsurface volumes of these contaminants.








Base from U.S. Geological Survey digital elevation data, 2006.



**EXPLANATION**

-  Hydrofacies model grid extent
-  Urban area
-  Boundary containing active area of local model



**Figure 1.** Study area near Modesto in the eastern San Joaquin Valley, California.

This study is part of the U.S. Geological Survey's (USGS) National Water-Quality Assessment (NAWQA) program. To improve understanding of the interrelationship between sources of contaminants, their transport through hydrologic systems, and the effects of contaminants and physical alterations on the quality of drinking water, a process-based study of the transport of anthropogenic and natural contaminants to public-supply wells (TANC) was initiated in 2001 (Wilber and Couch, 2002). The TANC study was designed to assess the vulnerability of public-supply wells to contamination by answering the question: "What are the primary anthropogenic and natural contaminant sources, aquifer processes, and well characteristics that control the transport and transformation of contaminants along flow paths to public-supply wells in representative water-supply aquifers?" The TANC study incorporates field data on solid-phase and water chemistry, geochemical analysis and interpretation, and process-based models to determine the vulnerability of public-supply wells to anthropogenic and natural contaminants at multiple scales and in multiple hydrogeologic settings across the nation. Results from the TANC study will provide a better understanding of the most important factors controlling the vulnerability of the nation's public-supply wells (Eberts and others, 2005).

Seven regional-scale (hundreds to thousands of km<sup>2</sup>) studies were completed in a range of settings using regional ground-water flow models and water-quality data from public-supply wells (Paschke and others, 2007) to evaluate aquifer hydrogeologic processes, well characteristics, and potential contaminant sources affecting the vulnerability of public-supply wells. Following the regional analysis, more detailed local-scale (less than 100 km<sup>2</sup>) studies were implemented in 4 of the 7 study areas: the Central Valley Aquifer System in the eastern San Joaquin Valley near Modesto, California, the Floridan Aquifer System near Temple Terrace, Tampa Bay Region, Florida, the Glacial Aquifer System near Woodbury, Connecticut, and the High Plains Aquifer System near York, Nebraska. The local-scale studies incorporated nested local ground-water flow and transport models to enhance the understanding of specific physical and chemical processes affecting the vulnerability of public-supply wells in the regional aquifer.

## **Purpose and Scope**

This report is one of two reports that document the local TANC study near Modesto in the eastern San Joaquin Valley, California ([fig. 1](#)). The results of the characterization of the hydrogeologic setting, water and solid-phase chemistry, and the geochemical analysis of processes affecting long-term concentrations of nitrate and uranium in a selected

public-supply well will be presented in a future report. The report presented here documents the development and calibration of the steady-state local ground-water flow model used in the analysis of the transport of nitrate and uranium to the public-supply well, and documents the results of the transport analyses. The hydraulic conductivity distribution of the aquifer system was generated using a conditional indicator geostatistical method. The local flow model was calibrated to water-level measurements from multilevel monitoring wells and to inflows and outflows from the regional model. Particle tracking analysis was used to delineate the contributing recharge area and the zone of contribution of the selected public-supply well and the monitoring wells in the study area. Concentrations of tracers computed using particle pathlines and associated flow were compared with measured concentrations of age-dating tracers collected in the wells. Particle ages and land use in the contributing recharge areas of the wells were compared to measured concentrations to evaluate the effects of land use on measured concentrations. Simulated concentrations of nitrate and alkalinity were compared with measured concentrations to evaluate the downward movement of nitrate and uranium in the aquifer. Future long-term concentrations of nitrate and uranium concentrations in the public-supply well were estimated using the calibrated local flow and transport model.

## **Description of Study Area**

The San Joaquin Valley occupies the southern two-thirds of the Central Valley of California ([fig. 1](#)), a large, northwest-trending, asymmetric structural trough filled with marine and continental sediments up to 10 km thick (Page, 1986; Gronberg and others, 1998). The San Joaquin Valley is a level depression more than 400 km long and 30 to 90 km wide. East of the valley, the Sierra Nevada rise to an elevation of more than 4,200 m; west of the valley are the Coast Ranges, a series of parallel ridges of moderate elevations (Mendenhall and others, 1916).

## **Hydrogeologic Setting**

Streams in the northern part of the San Joaquin Valley drain through the San Joaquin River northward; the southern part of the valley is hydrologically closed. The climate is semiarid, characterized by hot summers and mild winters, with rainfall primarily during late fall through early spring. Rainfall averaged 315 mm annually from 1931 to 1997 (National Oceanic and Atmospheric Administration, 2005).

The TANC regional-scale study area is about 2,700 km<sup>2</sup> in the northeastern San Joaquin Valley bounded on the west by the San Joaquin River, on the north near the Stanislaus River, on the south near the Merced River, and on the east by the Sierra Nevada foothills (Phillips and others, 2007a) (fig. 1). The San Joaquin River is the central drainage for the northern San Joaquin Valley and is the only major surface-water outlet from the valley. The Stanislaus, Tuolumne, and Merced Rivers drain the Sierra Nevada and are tributaries to the San Joaquin River. All rivers in the study area have been significantly modified from natural conditions. Each has multiple reservoirs for irrigation and power generation, which effectively delays discharge of large amounts of snowmelt runoff and reduces the peak discharge. Imprinted over this hydrology is an extensive network of canals used to deliver water for irrigation.

The local-scale study area that is the subject of this report is nested within the regional study area, occupying about 100 km<sup>2</sup> on the north side of Modesto (fig. 1). The local study area is situated on a belt of coalescing fluvial fans of low relief that lie between the dissected uplands to the east and the nearly flat surface of the valley floor (Burow and others, 2004). The sediments were deposited by the Stanislaus and Tuolumne Rivers as a heterogeneous mixture of unconsolidated, interlayered lenses of gravel, sand, silt, and clay (Marchand and Allwardt, 1981; Burow and others, 2004). Most of the unconsolidated deposits in the study area are contained within the Pliocene-Pleistocene Laguna, Turlock Lake, Riverbank, and Modesto Formations. The Turlock Lake, Riverbank, and Modesto Formations form a sequence of overlapping terrace and alluvial fan systems (Davis and Hall, 1959; Marchand and Allwardt, 1981) indicating cycles of alluviation, soil formation, and channel incision that were influenced by climatic fluctuations and resultant glacial stages in the Sierra Nevada (Bartow, 1991; Weissmann and others, 2004).

## Land and Water Use

Irrigated crops are planted in about 65 percent of the regional study area. Dominant crops include almonds, walnuts, peaches, grapes, grain, corn, pasture, and alfalfa. The local study area contains about 54 percent urban land and 46 percent agricultural land. The two most dominant crops are almond and fruit orchards. Agricultural irrigation began in the regional study area in the early 1900s and accounts for about 95 percent of the total water use. Surface-water supplies from the Stanislaus and Tuolumne Rivers are managed by irrigation districts and delivered to agricultural users through hundreds of kilometers of lined canals. Most irrigation districts and private agricultural users pump ground water for irrigation. Private agricultural ground-water pumpage is not measured in the regional or local study area, but is estimated as about 32 percent of total agricultural water use in water year 2000 (Burow and others, 2004; Phillips and others, 2007b).

During the last several decades, urban areas have expanded into the agricultural area as a result of increasing

population. In Stanislaus County, the estimated population in 2005 was more than 500,000 people, an increase of more than 10 percent since 2000 (California Department of Finance, 2006). Urban water demand is met by surface-water and ground-water supplies. Before 1995, the city of Modesto used ground water exclusively for public supply. In 1994, a surface-water treatment plant was completed. About 55 percent of Modesto's municipal and industrial water requirement was met with ground water in water year 2000 (Burow and others, 2004; Phillips and others, 2007b).

## Ground-Water Flow System

Ground water in the local study area is unconfined, although water-bearing layers of sand and gravel become semi-confined with depth owing to numerous, overlapping, discontinuous clay lenses. Before development of the ground-water resource, most ground-water recharge occurred in the upper parts of the alluvial fans where streams entered the basin. Ground water generally moved southwest, toward the axis of the San Joaquin Valley and discharged primarily to the San Joaquin River and surrounding marshlands (Gronberg and others, 1998). However, the diversion of surface water from streams, and intensive ground-water pumping and recharge resulting from irrigated agriculture and growth of the urban areas, have significantly altered the natural flow system. Following development of the ground-water resource, percolating irrigation water became the primary form of ground-water recharge, and irrigation pumpage became the primary form of ground-water discharge (Davis and others, 1959; Page and Balding, 1973; Londquist, 1981). As a result, ground water primarily moves downward within the regional and local flow systems. Water moving laterally may be pumped and reapplied at the surface multiple times. In addition, because ground-water recharge in the Modesto urban area is less than recharge in the agricultural areas, municipal ground-water withdrawals have created a water-level depression beneath the city (Burow and others, 2004).

The USGS installed several multi-depth monitoring wells in the regional study area near Modesto and near the Merced River (Phillips and others, 2007b). Monitoring wells were instrumented with pressure transducers that recorded hourly water-level measurements for periods typically ranging from 1 to 3 years. These data for the Modesto area show that vertical hydraulic gradients from the water table (about 10 m deep) to the deeper production zones of most municipal wells (about 40–100 m) were strongly downward during the spring and summer months (about 0.2–0.3). The downward gradient was weaker during the fall and winter. Seasonal water-level fluctuations are about 6 m in the deeper wells, and usually less than 1 m at the water table, in the Modesto area.



## Ground-Water Quality in Modesto Public-Supply Wells

The chemistry of ground water in the regional study area has been affected by agricultural and urban activities. Nitrate concentrations in public-supply wells in the Modesto area ranged from 0.23 to 9.5 mg/L, with a median of 3.5 mg/L during 1999–2000 (Wright and others, 2004). Nitrate concentrations were higher in public-supply wells on the periphery of the city than in wells near the center of the urban area. The wells containing higher nitrate concentrations were located in newer suburban developments, on previous agricultural land and closer to current agricultural areas where nitrogen fertilizers are used. Nitrate concentrations in shallow ground water beneath almond orchards, one of the dominant crops in the local study area, are typically high (Burow and others, 1998). In addition to anthropogenic nitrate concentrations, naturally-occurring trace elements and radionuclides in ground water, such as arsenic and uranium, are also of concern in the Modesto area. Uranium concentrations were above the MCL of 30  $\mu\text{g/L}$  in several public-supply wells, causing the abandonment of these wells for use (City of Modesto, written commun., 2003).

## Public-Supply Well Selection

A single public-supply well was selected for study at the local scale to evaluate the dominant processes affecting the vulnerability of public-supply wells in the Modesto area. The selection of the public-supply well for the local study was based on previous work at the regional scale that defined baseline hydrologic data and typical ground-water chemistry within the regional ground-water flow model domain.

The regional ground-water flow model was used to simulate the zone of contribution (ZOC) and the contributing recharge area (CRA) for 60 of 112 public-supply wells operating in the Modesto area (Phillips and others, 2007a). The CRA is defined as the areal extent at the water table (or top boundary) where water entering the ground-water flow system will eventually be removed by the discharging well. The ZOC is the three-dimensional volumetric part of the aquifer system through which ground water flows to the discharging well from the CRA (Focazio and others, 2002). Particle-tracking analysis was used to compute the extent and percentages of different land uses within the CRA of each well and to relate the contaminants in the wells to that land use.

The public-supply well selected for this study is in northeast Modesto (fig. 2), and was selected from a subset of 15 of the 60 wells for which CRAs were computed and for which water-quality samples were collected by the USGS in 2003. These 15 wells supplied the top 25 percent of annual pumpage in 2000, which ranged from 0 to 5,800  $\text{m}^3/\text{d}$  (1.5 Mgal/d). The public-supply well selected for study is one of the highest in annual production (1.2 Mgal/d; top 5 percent

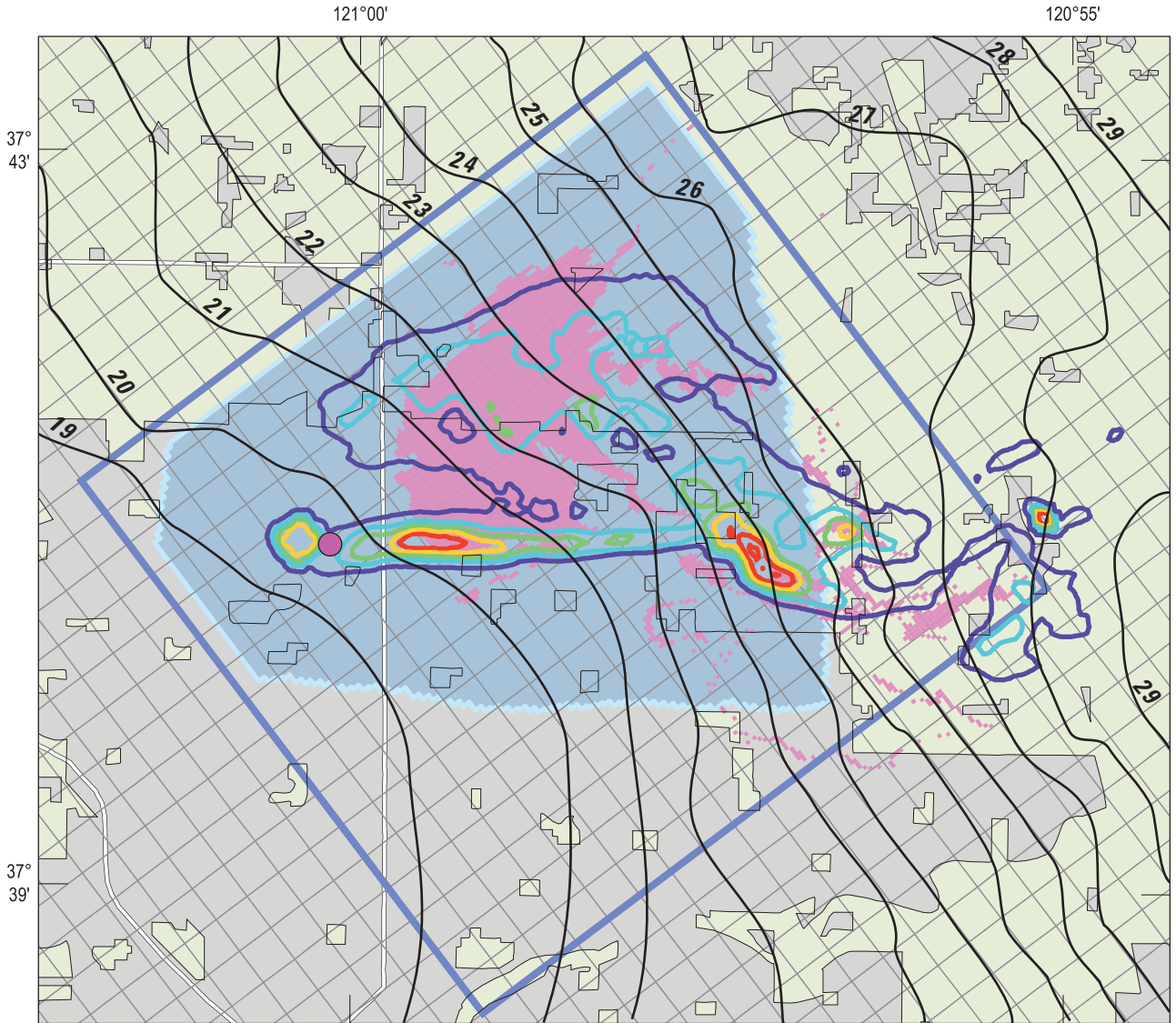
of total supply) and pumps at a rate of 6.1  $\text{m}^3/\text{min}$  (1,600 gal/min) during the summer season. In the winter, the well is pumped for a short duration every day, averaging 0.4  $\text{m}^3/\text{min}$  (110 gal/min) over a 24-hr period. The median well depth of public-supply wells in the Modesto area is 81.7 m (268 ft) and the median screened interval length is 27.7 m (91 ft), although many wells have no screened-interval information or have an open bottom. The public-supply well selected for this study is 120 m deep and is screened from 27.7 to 111.6 m below land surface and has an open bottom from 111.6 m to about 115 m. Of the 60 public-supply wells for which CRAs were computed, 45 percent had a CRA consisting of mostly urban land, 28 percent had a CRA consisting of mostly agricultural land, and 27 percent had a CRA consisting of a mixture of agricultural and urban land. To select the single public-supply well for this study, preference was given to wells that had a CRA that allowed the differences between agricultural and urban land-use effects on ground-water quality to be studied and the influence of urbanization on the quality of ground water reaching public-supply wells to be evaluated. The CRA computed for the selected well had an areal extent of 96  $\text{km}^2$  (fig. 2), containing about 65 percent agricultural land and 32 percent urban land (Phillips and others, 2007a). The well was constructed in 1961. Residential development began near the well in the 1960s and has expanded outward to the north and east.

The public-supply well selected for this study is deeper, has a longer screened interval, and is a larger producer than most wells in the Modesto area. This well was selected because it was screened across a large thickness of the aquifer system, and ground-water quality in the ZOC was expected to represent a transition from agricultural to urban land use. By characterizing the ground-water age and the processes affecting the water chemistry at different depths in the aquifer system, results can be extrapolated to other wells that are screened at shallow depth intervals.

## Ground-Water Flow Model

Movement of water and solutes from recharge areas to the public-supply well was evaluated using a steady-state, three-dimensional, ground-water flow and transport model (Pollock, 1994; Harbaugh and others, 2000). The local model developed for this study was nested within the regional model used for the TANC regional analysis in the northeastern San Joaquin Valley (fig. 2) (Paschke and others, 2007; Phillips and others, 2007a). Simulations of quantities of water of different ages and solute concentrations in the well provided information on ground-water velocities to complement the interpretation of water chemistry data from wells sampled for this study and provided estimates of long term nitrate and uranium concentrations in ground water in the study area.





Base from U.S. Geological Survey digital data, 2006.



**EXPLANATION**

- Contributing recharge area for travel times less than or equal to 100 years; derived from regional model pathline analysis
- Regional model grid
- Agricultural land use area
- Urban land use area
- Boundary containing active area of local model
- Simulated water-table elevation from regional model—  
Contour interval 1 meter. Datum is North American Vertical Datum of 1988
- Hydrofacies model grid extent
- Lines of equal particle density, in number of particles per model cell
  - less than or equal to 500
  - 501 to 1,000
  - 1,001 to 1,500
  - 1,501 to 2,000
  - more than 2,000
- Road or highway
- Public-supply well

**Figure 2.** Extent of local ground-water flow model nested within regional model of an area near Modesto, eastern San Joaquin Valley, California. Particle density map and contributing recharge area computed using regional model.

## Regional Ground-Water Flow Model

The regional ground-water flow model of the northeastern San Joaquin Valley used to provide stresses and boundary conditions for the local model was documented as part of the TANC regional-scale studies (Phillips and others, 2007a). The regional model grid is oriented parallel to the valley axis, 37 degrees west of due north (fig. 2). The model area extends 61.2 km along the valley axis and 54.8 km from the Coast Ranges to the Sierra Nevada foothills (fig. 1), though the area west of the San Joaquin River is inactive. Each model cell is 400 m by 400 m, and the grid has 153 rows and 137 columns. The regional model layering is a series of wedges that generally represent the regional dip of the sediments toward the southwest. Sixteen model layers were defined. Above the Corcoran Clay (a regional confining unit west of the local model area), model layer thickness ranged from 0.5 to 16 m; below the Corcoran Clay, model layer thicknesses ranged from 20 to 74 m. Layer thicknesses generally were designed to increase with depth and decreasing availability of sediment texture data. The top of the uppermost model layer represents the land surface, and the bottom is a smoothed version of the land surface. The thicknesses of layers 2 through 7 were assigned as a percentage of the thickness of materials between layer 1 and the top of the Corcoran clay. Layer 8 represents the Corcoran Clay where present; the top surface of the Corcoran Clay was a smoothed rendition constrained by data from driller's logs. The thickness of the Corcoran Clay ranged from 3 to 43 m. A thickness of 5 m was specified in layer 8 in the eastern part of the regional model where the Corcoran Clay was not present. The thicknesses of layers 9-16 were assigned as a percentage of the thickness of materials between the bottom of the Corcoran Clay and the bottom of the model. The total thickness of the wedge-shaped model ranged from about 220 to 430 m. Hydraulic conductivity was distributed using a spatial correlation model of sediment texture (as percentage of coarse-grained texture). This method uses the estimated sediment texture for each model cell and a method of calibration which uses horizontal and vertical hydraulic conductivities to estimate each textural end member. A vertical gradient was imposed at the general head boundaries on the north, south, and eastern sides of the model.

The regional model was refined during the development of the local model (Phillips and others, 2007b). Refinements included the following: (1) a three-dimensional model of percentage of coarse-grained texture to represent the spatially varying hydraulic conductivity field in the model domain (Burow and others, 2004) was incorporated, replacing the two-dimensional version; (2) the top and bottom surface and the extent of the Corcoran Clay were refined with additional data; (3) recharge was reduced as a result of continued analysis of the water budget data; (4) continuous water-level data available from the local study were used to improve calibration results (Phillips and others, 2007b).

## Local Ground-Water Flow Model

A three-dimensional, steady-state model of ground-water flow in the local study area was developed using MODFLOW-2000 (Harbaugh and others, 2000) to simulate movement of water in the contributing area of the public-supply well and to support the transport modeling analysis. The local model simulates conditions that existed in water year 2000, the period simulated by the regional steady-state model. Measured ground-water levels in the regional study area suggest that the ground-water system has been in a quasi-steady-state condition for many years (Phillips and others, 2007a). Although water levels rose rapidly in the Modesto area in 1995 after surface water was imported to supplement ground-water supplies for drinking water, the rise slowed greatly by 2000 (Burow and others, 2004). For the purposes of this study, the quasi-steady-state condition of the aquifer system is adequately represented by a steady-state model.

## Model Geometry and Discretization

The extent of the local ground-water flow model presented in this report encompasses the ZOC and CRA for travel times less than or equal to 100 years (fig. 2) as determined by particle pathline analysis using the regional model (Phillips and others, 2007a). As in the regional model, the local model grid is oriented parallel to the valley axis, 37 degrees west of due north (fig. 2), aligned with the regional lateral ground-water flow direction. The nested, local model was discretized into a uniform grid of finite-difference cells consisting of 200 rows of 72-m-length-cells and 100 columns of 34-m-length-cells.

The active area of the local model grid encompasses most of the CRA generated using the MODPATH particle-pathline analysis of the regional model (Phillips and others, 2007a) (fig. 2). In addition, a probabilistic method was used to evaluate the effect of parameter uncertainty on the CRA generated using the regional model. The probabilistic method uses a Monte Carlo technique which varies the hydraulic conductivity of geologic units in the model within the range of uncertainty. Nearly 700 parameter sets were generated using a covariance matrix for the optimal parameters, which were determined using a method of parameter estimation. Particles were tracked backward from the public-supply well for each of the 370 cases for which mass balance errors were less than 10 percent (Jeff Starn, U.S. Geological Survey, written commun., 2004). A larger number of model runs would provide more cases with lower mass balance error; however, computation time would be impractical. The local model was unaffected by the results of the probabilistic CRA, as it was generated primarily to determine the extent of the local model and help place monitoring wells for the local study. The combined particle endpoint distribution is mapped as contours of particle density (fig. 2). The CRA derived from the MODPATH particle-pathline analysis and the particle density

contours indicated that most of the recharge contributing to the public-supply well was east and north of the well; the highest density of particles was due east of the public-supply well.

The local model grid has 200 layers of uniform 0.6 m thickness. The active area of the model coincides with the water table at the top of the model and the bottom of the regional-scale model layer 10 at the bottom of the model, which is below the bottom of the public-supply well and below the dominant pumping zone in this area.

## Boundary Conditions, Model Stresses, and Initial Conditions

A mixture of specified head and specified flux boundaries were used to constrain the local model using head and flux values from the regional model (fig. 3). A series of model runs using different combinations of specified head and flux boundaries determined the best combination of boundary conditions. The resulting combination of boundaries was selected on the basis of residuals between measured and simulated water levels, model mass balance, and flow through boundaries and multi-node wells. Conditions along the north and south boundaries of the local model, representing approximate flow lines, were simulated using specified flux cells. Although these lateral boundaries approximated flow lines at the water table, flow directions varied with depth; therefore, lateral boundary conditions in the local model were specified fluxes derived from lateral flows simulated in the regional model. Cell-by-cell boundary fluxes for the local model were calculated from adjacent larger cells in the regional model by using a hydraulic-conductivity-weighted distribution. Net flows specified along the north and the south boundaries were 3,773 and  $-2,159$  m<sup>3</sup>/d, respectively, approximately an order of magnitude lower than the net flows through the upgradient and top (recharge) boundaries. The upgradient and downgradient lateral boundaries were specified head, using values from the regional model. Hydraulic head varied from 26 m near the water table to 16 m at depth along the upgradient boundary, whereas hydraulic head varied from 19 m near the water table to 13 m at depth along the downgradient boundary. The hydraulic head values were interpolated from the regional model onto the local model grid. The lower boundary of the local model was specified head from the regional model; hydraulic heads from the regional model were interpolated onto the local model grid in the same way as the lateral boundaries. The upper boundary of the local model was specified flux to represent the water table.

Stresses in the local model include recharge and ground-water withdrawal from wells. Recharge in the local model was derived from agricultural and urban water budget subareas

from the regional model (Burow and others, 2004; Phillips and others, 2007b). Recharge from agricultural return flow was estimated using the calculated crop demand in the regional water-budget analysis and an estimated consumptive use of applied water. Recharge in the urban area was estimated by accounting for landscape irrigation, leakage from water distribution lines, and precipitation recharge. Recharge rates from the regional model ranged from 0.6 to 0.7 m/yr in the agricultural areas, and were 0.3 m/yr in the urban areas. The recharge specified from the regional model was adjusted on a cell-by-cell basis during calibration of the local model to account for the heterogeneous hydraulic conductivity distribution used in the model, and limit mounding of hydraulic heads in low-permeability cells (fig. 3). In some cases, recharge applied to cells moved laterally and discharged from adjacent cells because of the local geometry of the hydraulic conductivity distribution. However, the total amount of recharge and the approximate ratio of agricultural (67 percent) to urban (33 percent) recharge specified in the regional model was maintained as much as possible.

Total ground-water pumpage assigned in the local model was 49,822 m<sup>3</sup>/d, distributed among 22 wells (table 1). Private agricultural ground-water pumpage was not measured in the regional study area, but was estimated in the water budget analysis for the regional model (Burow and others, 2004; Phillips and others, 2007b). The locations of privately pumped wells also are unknown; therefore, agricultural pumpage was distributed areally within the agricultural water budget subarea by assuming an average well spacing of 1,200 m. The vertical distribution of private agricultural pumpage was estimated using the average screened interval of irrigation wells in each subarea. Wells operated by irrigation districts or for public supply were assigned known pumping rates across documented screened locations. Pumping in 15 of the wells in the local model area was simulated using the standard well package in MODFLOW-2000 (fig. 3). Pumping in each model layer within the screened interval for each well was assigned by weighting the total pumpage by the hydraulic conductivity of each layer along the well screen. To account for potential flow vertically through the wellbore, pumping in 7 of the wells in the local model was simulated using the multi-node well package in MODFLOW-2000 (Halford and Hanson, 2002). To minimize model computation time, only wells containing long screened intervals were simulated as multi-node wells: wells were simulated as multi-node wells if the top of the screened interval was less than about 35 m below the water table, the bottom of the screened interval was deeper than about 80 m below the water table, and the screen length was greater than 50 m.



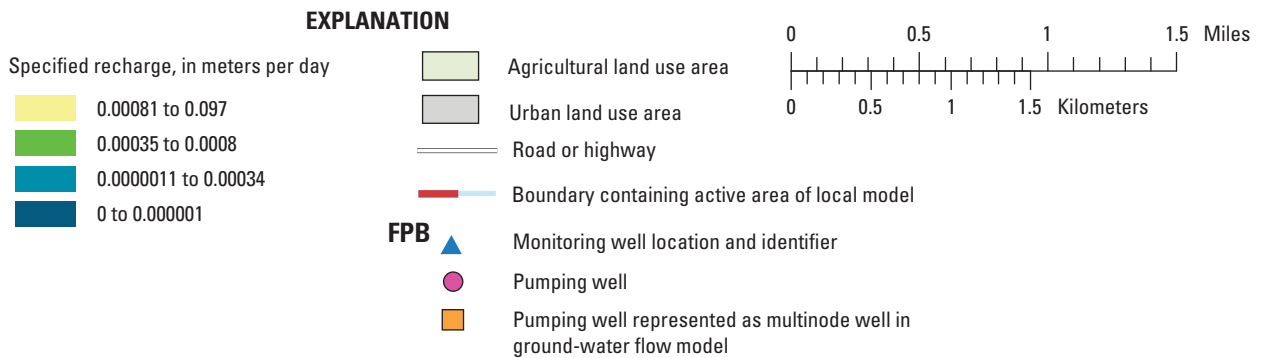
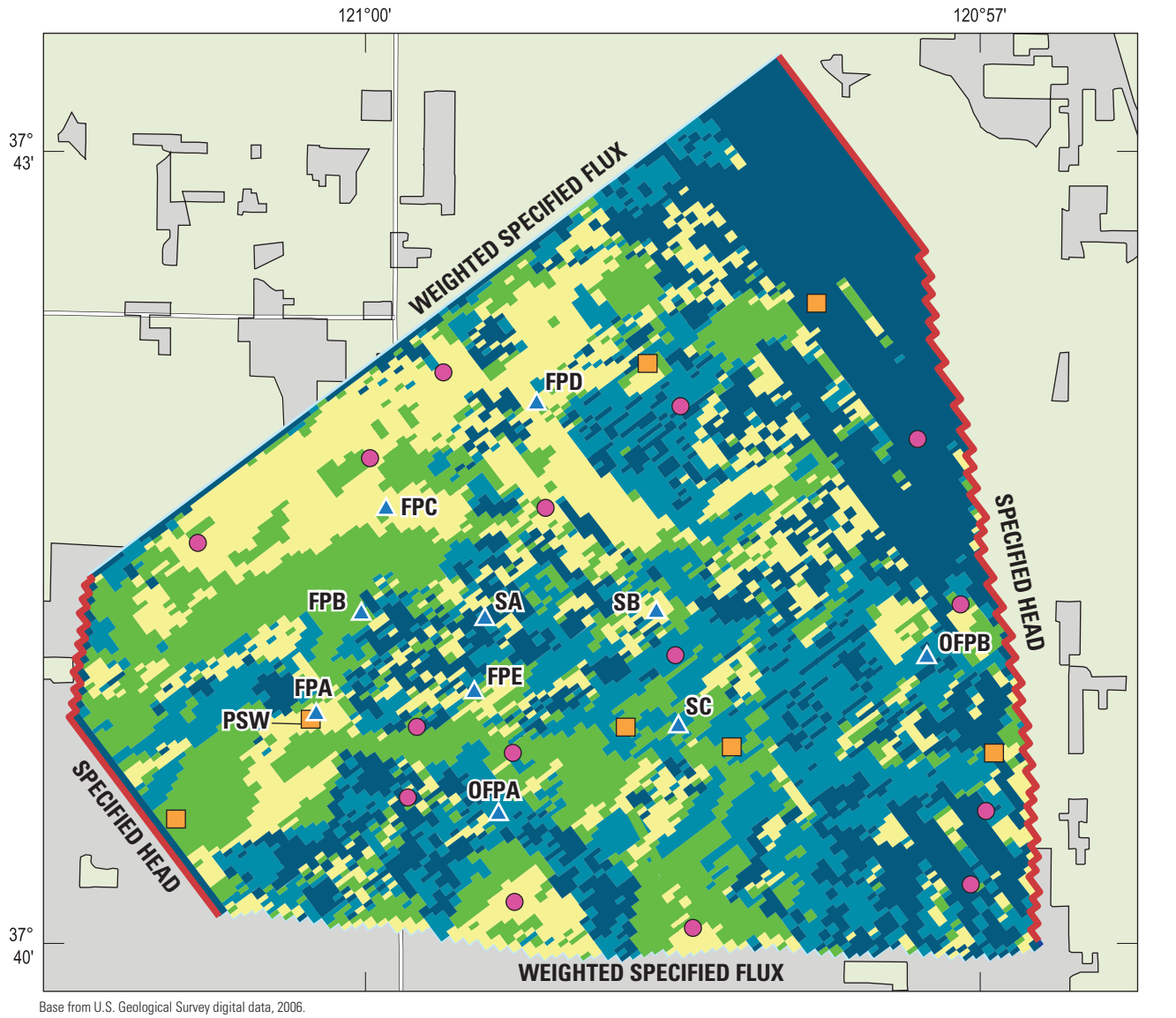


**Figure 3.** Boundary conditions and distribution of recharge specified in the local ground-water flow model near Modesto, eastern San Joaquin Valley, California. PSW, public-supply well.

**Table 1.** Well depths and pumping rates assigned to wells in the local ground-water flow model near Modesto, eastern San Joaquin Valley, California.

| Local well name                | Depth to top of screen below water table, in meters | Depth to bottom of screen below water table, in meters | Screen length, in meters | Pumping rate, in cubic meters per day |
|--------------------------------|---|--|--------------------------|---------------------------------------|
| A-206                          | 17.7  | 113.7  | 96.0                     | 206                                   |
| A-3A                           | 41.8  | 92.0   | 50.2                     | 3,607                                 |
| A-3B                           | 41.1  | 91.1   | 50.0                     | 3,607                                 |
| A-3C                           | 49.3  | 86.5   | 37.2                     | 3,607                                 |
| A-3D                           | 31.0  | 92.9   | 61.9                     | 3,607                                 |
| A-3E                           | 48.7  | 74.1   | 25.4                     | 3,607                                 |
| A-6A                           | 52.2  | 78.7   | 26.5                     | 3,078                                 |
| B-24                           | 14.0  | 95.7   | 81.7                     | 1,238                                 |
| B-25                           | 13.8  | 123.3  | 109.5                    | 3,746                                 |
| B-37                           | 13.5  | 60.9   | 47.4                     | 3,306                                 |
| B-39                           | 20.1  | 65.6   | 45.5                     | 4,206                                 |
| B-46                           | 24.5  | 66.8   | 42.3                     | 2,714                                 |
| B-48                           | 66.3  | 119.5  | 53.2                     | 2,542                                 |
| B-50                           | 44.1  | 94.7   | 50.6                     | 2,163                                 |
| B-52                           | 23.1  | 97.1   | 74.0                     | 4,327                                 |
| B-54                           | 39.5  | 129.4  | 89.9                     | 1,460                                 |
| B-58                           | 92.5  | 118.9  | 26.4                     | 204                                   |
| B-259                          | 11.8  | 91.5   | 79.7                     | 505                                   |
| B-260                          | 22.8  | 98.1   | 75.3                     | 603                                   |
| B-262                          | 69.2  | 95.3   | 26.1                     | 692                                   |
| B-264                          | 69.5  | 121.8  | 52.3                     | 344                                   |
| B-269                          | 41.7  | 91.6   | 49.9                     | 453                                   |
| Total pumpage from local model |   |  |                          | 49,822                                |

## Aquifer Hydraulic Conductivity

The distribution of hydraulic properties used in the local model was estimated by model calibration using a three-dimensional spatial correlation model of hydrofacies. The spatial correlation model of hydrofacies was developed using a transition-probability-based geostatistical approach to explicitly evaluate the effects of dispersion on solute concentrations in the aquifer caused by macro-scale heterogeneity. A single realization (a plausible three-dimensional representation of the hydrofacies distribution) of the distribution of hydrofacies was selected from a series of realizations and used to calibrate the flow model. Hydrofacies are defined here as sediments with similar hydraulic properties that were deposited in similar depositional environments. Using this approach, the three-dimensional character of the movement of water through primary channels is preserved, and more accurately represents transport pathways and dispersion of contaminants moving to the well.

Hydraulic conductivity was specified for each model grid cell using a stochastically-generated hydrofacies distribution. The hydrofacies distribution was generated using a conditional indicator geostatistical method that uses a transition-probability Markov-chain model to define the statistical

correlation structure of discrete hydrofacies (Carle and Fogg, 1996, 1997; Carle 1997; Carle and others, 1998). A matrix of transition probabilities was developed for the dip, strike, and vertical directions. From the transition rate matrices, a continuous lag Markov Chain model was developed, which was used with cokriging in a sequential indicator simulation to generate images of subsurface facies distributions. The hydrofacies distribution was generated using the software TProGS (Carle, 1999).

## Hydrofacies Classification

The alluvial sediments in the local study area consist primarily of interlayered lenses of gravel, sand, silt, and clay deposited in alluvial fans by the Stanislaus and Tuolumne Rivers (Jurgens and others, in press). The sediments were deposited in cyclic alluvial fan aggradation sequences linked to Pleistocene glacial episodes and the local base level of the San Joaquin River (Davis and Hall, 1959; Weissmann and others, 2002; Burow and others, 2004; Weissmann and others, 2004). For this study, sediments were classified into four hydrofacies: gravel, sand, muddy sand, and mud. The term mud is defined here as undifferentiated silt and (or) clay. The gravel hydrofacies is characterized as cobbles and pebbles in a coarse sand matrix, representing channel lag deposits, and has the highest hydraulic conductivity. The sand hydrofacies is characterized as moderately-well sorted medium to coarse sand, deposited in primary channels of the Stanislaus and the Tuolumne Rivers or secondary tributary channels. The muddy sand hydrofacies is characterized as finely laminated fine-grained sand in a matrix of clay and silt, deposited in the floodplain proximal to channels. The mud hydrofacies is characterized as massive to laminated silt and mud, deposited in the floodplain farther from the channel than the muddy sand hydrofacies and has the lowest hydraulic conductivity. The hydrofacies categories were based on previous classification of deposits on the Kings River alluvial fan (Burow and others, 1997; Weissmann and Fogg, 1999). The sediments in the study area are similar to the Kings River alluvial fan sediments because they were derived from similar source rocks and deposited by similar processes. The Tuolumne River and Kings River fans have similar drainage basin sizes, stream gradients, and changes in elevation; the Stanislaus River fan has a smaller drainage-basin size. All three drainage basins were extensively glaciated. The Stanislaus and the Tuolumne River alluvial fans are smaller than the Kings River fan, however. The basin subsidence rates near the Stanislaus and Tuolumne Rivers are significantly lower and the basin width is significantly smaller than that near the Kings River (Weissmann and others, 2004). Therefore, the paleosol hydrofacies in the Kings River fan (Weissmann and Fogg, 1999) is not well preserved in the study area and therefore was not included as a separate facies.

### Spatial Correlation Model of Hydrofacies

To develop the three-dimensional spatial correlation model of hydrofacies, sediment descriptions derived from continuous core collected by the USGS at site MREA (fig. 1) and from cuttings and e-logs obtained during drilling for the TANC study were discretized into 0.3-m increments and assigned a hydrofacies category. The transition probability matrix for the vertical direction was developed by fitting a Markov Chain model to the discretized data and using the calculated proportions of each hydrofacies category. Calculated proportions were 0.01, 0.19, 0.31, and 0.49 for gravel, sand, muddy sand, and mud hydrofacies, respectively.

Core and cuttings data were too sparse in the lateral directions to develop the Markov Chain model in the strike and dip directions by the same data fitting procedure. Transition probability matrices for the strike and dip directions were developed by using the calculated proportion of each hydrofacies and by modifying parameters used in Weissmann and Fogg (1999). Because the Tuolumne River alluvial fan is about half the area of the Kings River alluvial fan, the correlation lengths of the hydrofacies were reduced by a factor of about 2 to represent the difference in scale between the two fans.

The Markov Chain model developed from the transition probability matrices (table 2) was used in a conditional sequential indicator simulation to generate multiple equiprobable realizations. Separate realizations of the hydrofacies distributions were generated for each of six aggradation sequences (Jurgens and others, in press) to reflect the unconformities produced by extensive periods of non-deposition or erosion (Weissmann and Fogg, 1999). The resulting realizations were combined to represent the three-dimensional hydrofacies distribution for use in the local ground-water flow model.

Eleven sets of realizations were generated for each of the combined alluvial fan aggradation sequences. Each resulting hydrofacies distribution was used in preliminary ground-water

flow simulations to determine which distribution best fit the measured water levels. None of the model simulations using the eleven sets of realizations matched the magnitude of the vertical hydraulic gradient of about 0.075 (annual average) measured between depths of about 35 and 55 m below land surface. This depth interval corresponded to a fine-grained zone observed in borehole cuttings and geophysical logs at this depth. Therefore, a more continuous mud layer about 6 m thick was generated by increasing the correlation length of the mud hydrofacies at these depths. The ground-water flow model was run for each of the 11 realizations using 2 different mud layers, for a total of 22 model runs. The realization that best fit measured water levels was selected for subsequent ground-water flow model calibration and transport modeling (fig. 4A,B).

### Ground-Water Flow Model Calibration

The local flow model was calibrated using formal parameter estimation and systematic manual calibration techniques. Preliminary calibration was done using the parameter estimation process in MODFLOW-2000 (Hill and others, 2000) by comparing simulated and measured water levels. Because the estimated parameters were significantly correlated and because it was difficult to automate the updating of the hydraulic-conductivity-weighted flux boundaries during each parameter estimation run, the parameter estimation method was used to provide preliminary estimates of hydraulic conductivity of the hydrofacies. The hydraulic conductivity values were later refined through a systematic manual calibration. The head-based calibration was further evaluated by comparing fluxes in the regional model and comparing proportions of recharge in the urban and agricultural areas.

**Table 2.** Embedded transition probability matrices and mean hydrofacies lengths in the geologic model near Modesto, eastern San Joaquin Valley, California.

[L, mean length of hydrofacies, in meters; s, symmetry assumed; b, background category; <, less than]

|                   | Vertical direction |         |            |         | Horizontal strike direction |         |            |         | Horizontal dip direction |                   |            |         |         |      |
|-------------------|--------------------|---------|------------|---------|-----------------------------|---------|------------|---------|--------------------------|-------------------|------------|---------|---------|------|
|                   | Gravel             | Sand    | Muddy sand | Mud     | Gravel                      | Sand    | Muddy sand | Mud     | Gravel                   | Sand              | Muddy sand | Mud     |         |      |
| <b>Gravel</b>     | L = 1.2            | 0.45    | 0.54       | 0.01    | <b>Gravel</b>               | L = 110 | 0.45       | 0.54    | 0.01                     | <b>Gravel</b>     | L = 370    | 0.45    | 0.54    | 0.01 |
| <b>Sand</b>       | <0.01              | L = 1.4 | 0.53       | 0.46    | <b>Sand</b>                 | s       | L = 300    | 0.53    | 0.38                     | <b>Sand</b>       | s          | L = 862 | 0.53    | 0.39 |
| <b>Muddy sand</b> | 0.06               | 0.4     | L = 2.0    | 0.54    | <b>Muddy sand</b>           | s       | s          | L = 190 | 0.75                     | <b>Muddy sand</b> | s          | s       | L = 450 | 0.80 |
| <b>Mud</b>        | 0.01               | 0.46    | 0.53       | L = 3.3 | <b>Mud</b>                  | b       | b          | b       | b                        | <b>Mud</b>        | b          | b       | b       | b    |

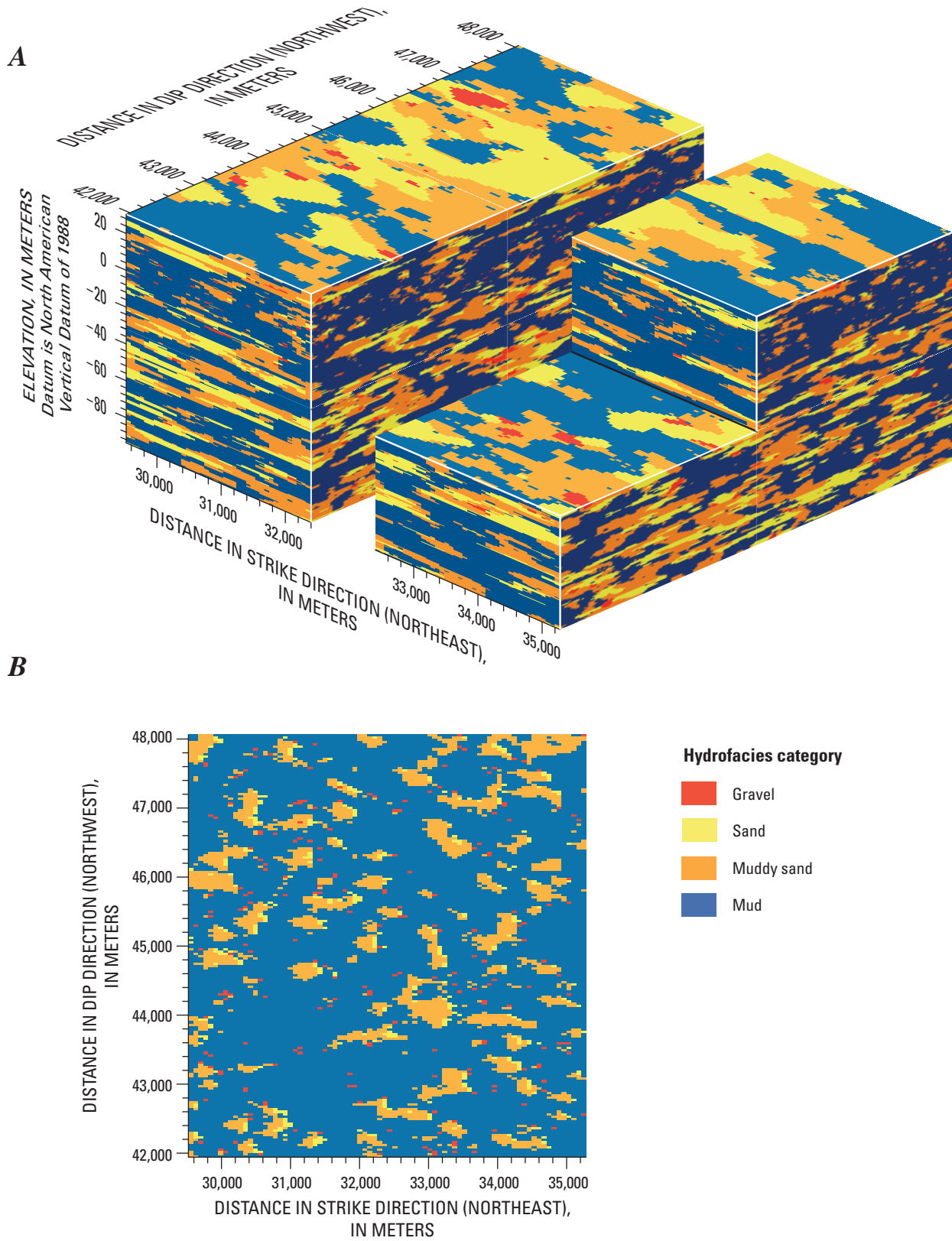


**Figure 4.** Hydrofacies distribution used in the ground-water flow model near Modesto, eastern San Joaquin Valley, California. (A) Three-dimensional model of hydrofacies and (B) two-dimensional view of clay 6 meters thick inserted at depths ranging from 35 to 55 meters below land surface.



Simulated water levels were compared to measured water levels in 18 monitoring wells screened at multiple depths at 7 sites (FPA, FPB, FPC, FPD, FPE, OFPA, and OFPB) (fig. 3). Measured water levels at sites SA, SB, and SC were not included in the calibration because these sites contained only water table wells, had a limited number of water-level measurements, and the water table elevation was represented at the other 7 sites. Water-level data for each well were averaged between the summer low period and the winter high period to determine the annual water-level observation. Water levels in the shallow part of the aquifer varied as much as 0.2 m seasonally, whereas water levels varied by as much as 5.6 m seasonally in the deep part of the aquifer because of seasonal changes in water demand. Water levels in the deep part of the aquifer were as much as 10 m lower than water levels in the shallow system during the summer months, however, indicating that the difference between water levels at the water table and the deep part of the aquifer is greater than the difference in water levels caused by seasonal changes.

Hydraulic conductivities were initially estimated using slug tests, aquifer tests, and results from previous investigations. Four hydraulic conductivity parameters were estimated during the calibration: the horizontal hydraulic conductivity of the sand hydrofacies (HK2), the horizontal and the vertical hydraulic conductivities of the muddy sand hydrofacies (HK3 and VK3, respectively), and the vertical hydraulic conductivity of the mud hydrofacies (VK4). Because the gravel hydrofacies represents only 1.4 percent of the modeled volume, simulation results were insensitive to changes in the hydraulic conductivity of that hydrofacies. Therefore, the initial estimate of hydraulic conductivity of the gravel hydrofacies was not adjusted. Similarly, the results were insensitive to the vertical hydraulic conductivity of the sand hydrofacies and the horizontal hydraulic conductivity of the mud hydrofacies, and therefore these values also were not further adjusted in the calibration process.

Initial model runs using the parameter estimation package resulted in estimated hydraulic conductivity values for the sand (HK2), muddy sand (HK3 and VK3), and mud hydrofacies (VK4) of 98, 2, 1, and 0.001 m/d, respectively. These estimates were generally at the high end of the range of expected hydraulic conductivity values for these hydrofacies (Freeze and Cherry, 1979; Domenico and Schwartz, 1998). The simulations were most sensitive to the vertical hydraulic conductivity of the mud hydrofacies (VK4). Although the simulations were least sensitive to the muddy sand hydrofacies parameters (HK3 and VK3), the muddy sand hydrofacies was expected to have the largest range of possible values. Some of the sediments in this hydrofacies were moderately well sorted, whereas some contained interstitial or laminated silt and clay, depending on the relative proximity to the channel during deposition. For subsequent calibration, muddy

sand hydrofacies parameters (HK3 and VK3) and vertical hydraulic conductivity of the mud (VK4) were adjusted through a manual calibration procedure. The hydraulic conductivity of the sand (HK2) was 98 m/d, within the range of values estimated in similar studies: the calibrated hydraulic conductivity for the 100-percent coarse-grained textural end-member in the regional model was 80 m/d (Phillips and others, 2007b); the estimated hydraulic conductivity of the sand hydrofacies in a local model nested within the same regional model was 80 m/d (Phillips and others, 2007b); the estimated hydraulic conductivity of the sand hydrofacies in a local model in an area north of Modesto was more than 130 m/d (Fleckenstein and others, 2006). The local studies used the same hydrofacies approach.

Because 7 of the 18 water-level measurements were in wells screened at the water table, the simulation results were primarily sensitive to hydraulic conductivity of the hydrofacies at the recharge boundary. Although the recharge flux applied from the regional model was weighted according to the hydraulic conductivity of the recharge cells, in some locations simulated water levels at the water table were highly variable and water mounded at cells insufficiently connected to high conductivity cells deeper in the model. In these cases, recharge applied to cells moved laterally and discharged from adjacent cells. To determine which recharge cells were best connected to high hydraulic conductivity cells in deeper parts of the model, the recharge boundary was specified as a constant-head boundary. The specified head approximated the water table from the regional model. Hydraulic conductivity values for the muddy sand hydrofacies (HK3 and VK3) were then systematically varied to obtain the best fit between simulated water levels and measured water levels while maintaining the approximate total flows derived from the regional model. A specified flux was then applied at the recharge boundary on the basis of the simulated fluxes from the specified head run. Resulting fluxes were distributed equally between the urban and the agricultural areas, which is inconsistent with relative recharge rates estimated from the water budget: about 66 percent of the recharge occurs in the agricultural area and 34 percent occurs in the urban area. Therefore, the recharge was redistributed by assigning a higher weight to the fluxes assigned in the agricultural area. The redistributed recharge was further refined by matching flows through the bottom, upgradient, and downgradient boundaries to flows from the regional model. Total recharge specified in the local model area was within 1.5 percent of the recharge from the regional model, with 58 percent of the recharge in the agricultural area and 42 percent in the urban area (fig. 3). Vertical hydraulic conductivity of the mud hydrofacies (VK4) was adjusted manually to obtain the best fit between simulated water levels and measured water levels for the given boundary conditions.



The final estimates of horizontal (HK3) and vertical (VK3) hydraulic conductivity for the muddy sand were 2.2 and 1.1 m/d, respectively (table 3). The final estimate of vertical hydraulic conductivity of the mud (VK4) was 0.0031 m/d, which was similar to 0.008 m/d, the calibrated hydraulic conductivity for the 0-percent coarse-grained textural end-member (fine grained) in regional model (Phillips and others, 2007b). These values are within the range of values from the literature (Bouwer, 1978; Freeze and Cherry, 1979; Domenico and Schwartz, 1998) and from the slug and aquifer test analyses. The resulting simulated water levels were generally similar to measured water levels, although they deviated at a few wells (fig. 5A), such as water table wells FPC-1 and FPD-1, intermediate-depth wells FPA-3, FPD-2 and OFPA-2, and the deepest monitoring well adjacent to the public-supply well, FPA-4. The sum of squared weighted residuals between simulated and measured water levels was 9.3 m<sup>2</sup>; the average residual was 0.25 m. Ten of the 18 water levels were within 0.5 m of measured water levels. Weights were applied to measurements at site FPD because this site was influenced by an adjacent canal, and it was in the agricultural setting where the location of pumping wells was not known. The relation between simulated water levels and weighted residuals appears to be generally independent and normally distributed (fig. 5B), although the distribution appears slightly biased by the wells noted above. Simulated water levels were less than measured in 12 of 18 wells.

Local differences between simulated and measured water levels was likely due to a lack of correspondence between the realization selected for simulation and the true distribution of hydrofacies around individual wells. The

hydrofacies distributions were conditioned on hydrofacies data at the boreholes, but the degree of interconnection between high permeability hydrofacies adjacent to individual wells varied among realizations and was expected to influence the simulation of water levels at the well. Because the public-supply well is screened over a much greater thickness than the monitoring wells, the public-supply well was less affected by the local variations in hydrofacies distributions. The three-dimensional character of the movement of water through primary channels was preserved using this hydrofacies approach to characterizing the three-dimensional hydraulic conductivity distribution, and more accurately simulates transport pathways and dispersion of contaminants moving to the well.

Simulated vertical gradients were similar to measured vertical gradients. Simulated vertical gradients ranged from 0.04 to 0.07 between the water table and the deepest wells at each site, and measured vertical gradients ranged from 0.04 to 0.08. The simulated flows in the local model were similar to flows from the regional model (fig. 6). Net flow through the top (recharge) boundary and the upgradient (east) boundary was within 1.5 percent of the flow in the regional model. Net flow through the downgradient (west) boundary was lower than flow in the regional model, and net flow through the bottom boundary of the model was higher than the flow in the regional model, although the net flows through these boundaries were an order of magnitude less than flow through the upgradient and recharge boundaries.

**Table 3.** Hydraulic conductivity of hydrofacies used in the local ground-water flow model near Modesto, eastern San Joaquin Valley, California.

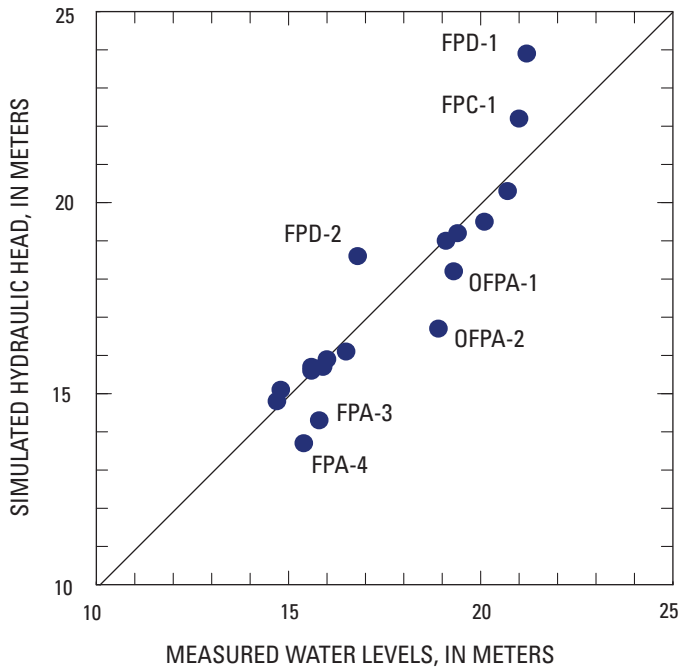
[ —, not enough data]

| Hydrofacies       | Horizontal hydraulic conductivity used in simulation | Vertical hydraulic conductivity used in simulation | Minimum hydraulic conductivity from slug tests | Maximum hydraulic conductivity from slug tests | Average hydraulic conductivity from slug tests | Hydraulic conductivity from aquifer test | Range of literature values <sup>1</sup> |
|-------------------|--|--|--|--|--|--|---|
| In meters per day |  |  |  |  |  |  |   |
| Gravel            | 800  | 727  | 2  | 6  | 4  | 20                                       | 1 to 2,500                              |
| Sand              | <sup>2</sup> 98                                      | 45   | 2  | 24   | 8  | 20                                       | 0.01 to 500                             |
| Muddy sand        | <sup>2</sup> 2.2                                     | <sup>2</sup> 1.1                                   | 0.3  | 6  | 3  | 2  | 0.0001 to 20                            |
| Mud               | 0.001  | <sup>2</sup> 0.0031                                | 0.0006   | 6  | —  | 0.0004                                   | 1E-8 to 0.01                            |

<sup>1</sup>From Bouwer, 1978; Freeze and Cherry, 1979; Domenico and Schwartz, 1998.

<sup>2</sup>Estimated during calibration.

**A**



**B**

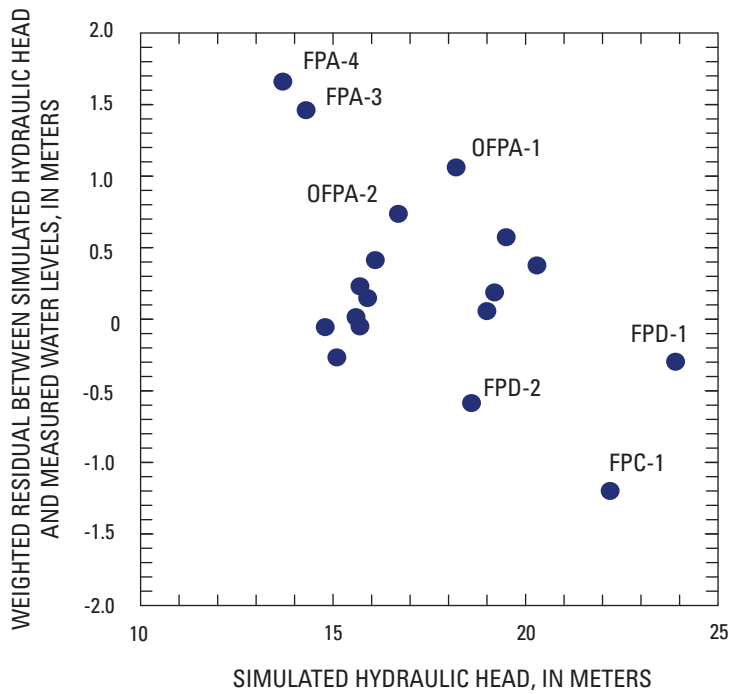


**Figure 5.** (A) Simulated and measured water level and (B) weighted residuals for the calibrated local ground-water flow model near Modesto, eastern San Joaquin Valley, California.

## Sensitivity Analysis

To determine the influence of model parameters on model results, the horizontal and vertical hydraulic conductivity of the sand (HK2 and HK3), the vertical hydraulic conductivity of the muddy sand (VK3), and the vertical hydraulic conductivity of the mud (VK4) were each varied independently over a range of 0.2 to 5 times their calibrated value. Recharge fluxes were held constant for the set of sensitivity runs. Model sensitivity is reported in terms of the sum of squared residuals between simulated and measured water levels (fig. 7A). Simulated water levels are most sensitive to VK4. Heads are matched more closely with higher HK2 values, although the improvement becomes less significant after 2 times the calibrated value. Because the sum of squared residual statistic may be dominated by the water levels at the water table, however, flows through the upgradient (east) and downgradient (west) specified head boundaries were also compared (figs. 7B,C). Simulated flows through the boundaries are most sensitive to HK2, followed by VK4. Both simulated water levels and flows are generally insensitive to changes in HK3 and VK3. The hydraulic conductivity and anisotropy of the muddy sand facies (HK3 and VK3) can vary widely, depending on whether the fine sands have interstitial or laminated silts and clay present, and the muddy sand facies is likely one of the least well-characterized hydrofacies (Dalgish, 2006). Sensitivity runs with constant anisotropy of 2 for HK3 and VK3 indicate that simulated water levels and flows were insensitive to changes in HK3 and VK3 (figs. 7A,B,C).

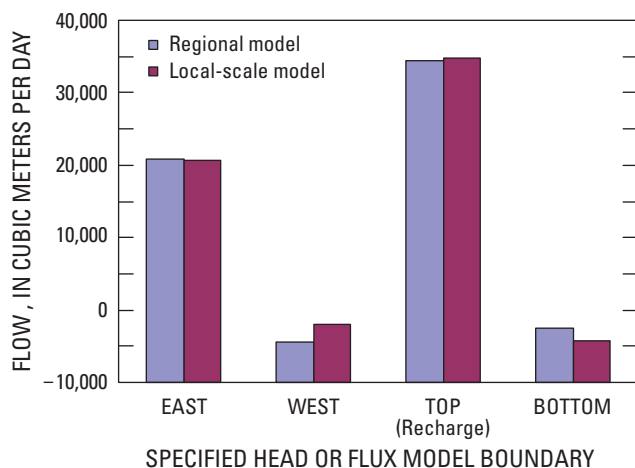


**Figure 6.** Comparison between boundary flows in the regional model and boundary flows in the calibrated local ground-water flow model near Modesto, eastern San Joaquin Valley, California. In the local model, east, west, and bottom boundaries are specified head and top boundary is specified flux.

## Ground-Water Flow Model Results

### Simulated Water Levels and Flows

The simulated water table (fig. 8) indicates that horizontal movement of ground water in the shallow part of the aquifer system generally is from north to south from the agricultural area toward the center of the urban area. The simulated horizontal hydraulic gradient was about 0.002. In contrast, horizontal movement of water at layer 150 (80–85 m below land surface) was generally from the northeast to southwest and had a horizontal hydraulic gradient of about 0.001 (fig. 9). The differences in horizontal flow direction between the shallow and the deep system are likely related to the distribution of pumping. Although only 14 percent of the total simulated withdrawals occurred in layers deeper than layer 150, 3 wells that each accounted for at least 10 percent and together totaled 59 percent of the withdrawals below layer 150 are in the northwest part of the model. The simulated and measured vertical gradients in the study area indicate that most ground water moves downward toward pumping well screens (fig. 10).

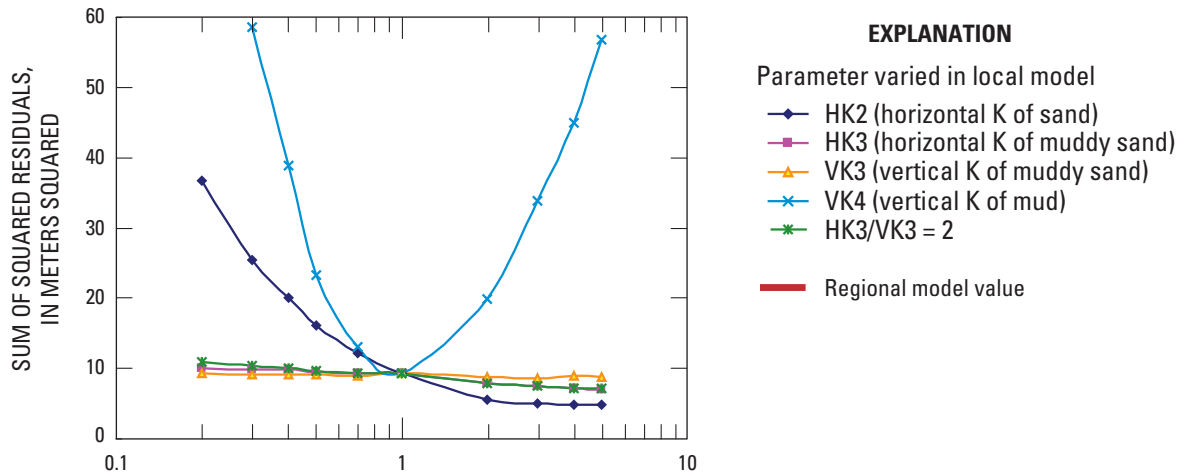
### Simulated Budget

The steady-state volumetric ground-water flow budget indicates the importance of recharge and pumping stress on the aquifer system (table 4). Total flow through the model was about 98,000 m<sup>3</sup>/d. Inflow through the upgradient and recharge boundaries accounted for 40 and 26 percent of the total inflow, respectively, whereas outflow through the wells accounted for 51 percent of the total outflow. The model was partially calibrated to flows from the regional model at specified head boundaries (fig. 6), so the resulting flows are strongly controlled by boundary conditions generated from the regional model.

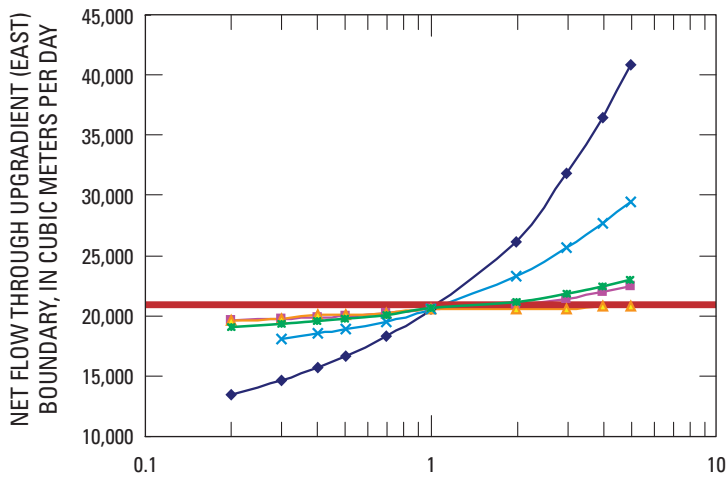
## Simulation of Advective Transport by Particle Tracking

Particle tracking was used to compute pathlines and advective travel times in the local ground-water flow model. The CRA and ZOC were delineated for the public-supply well and used to characterize the age and source of water reaching the well. Simulated travel times and recharge rates for the public-supply well and the monitoring wells were combined with estimated input concentrations for various tracers to calculate simulated flux-weighted concentrations reaching the wells. The simulated concentrations were compared to measured concentrations in the wells to evaluate the adequacy of model parameters. Long term concentrations of nitrate and uranium in the public-supply well were estimated using input concentrations for nitrate and alkalinity concentrations.

A



B



C

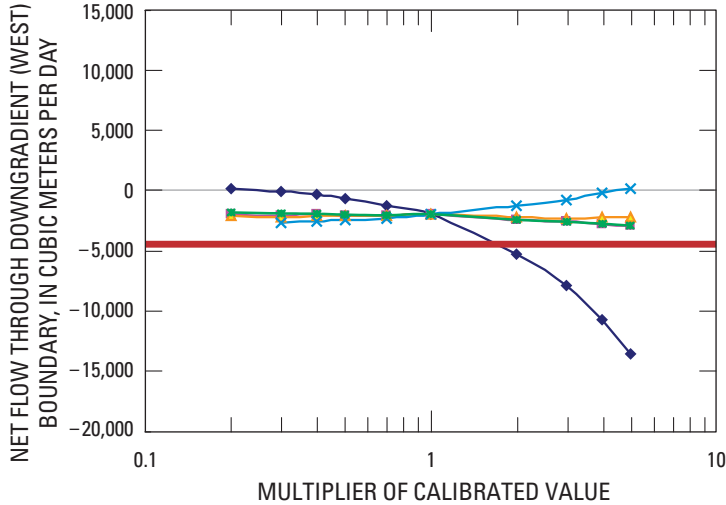


**Figure 7.** Sensitivity of model parameters with respect to (A) sum of squared residuals of simulated and measured water levels, (B) net flow through upgradient (east) boundary, and (C) net flow through downgradient (west) boundary. HK2, horizontal hydraulic conductivity of sand hydrofacies; HK3, horizontal hydraulic conductivity of muddy sand hydrofacies; VK3, vertical hydraulic conductivity of muddy sand hydrofacies; VK4, vertical hydraulic conductivity of mud hydrofacies; HK3/VK3, ratio of horizontal to vertical hydraulic conductivity for muddy sand hydrofacies.

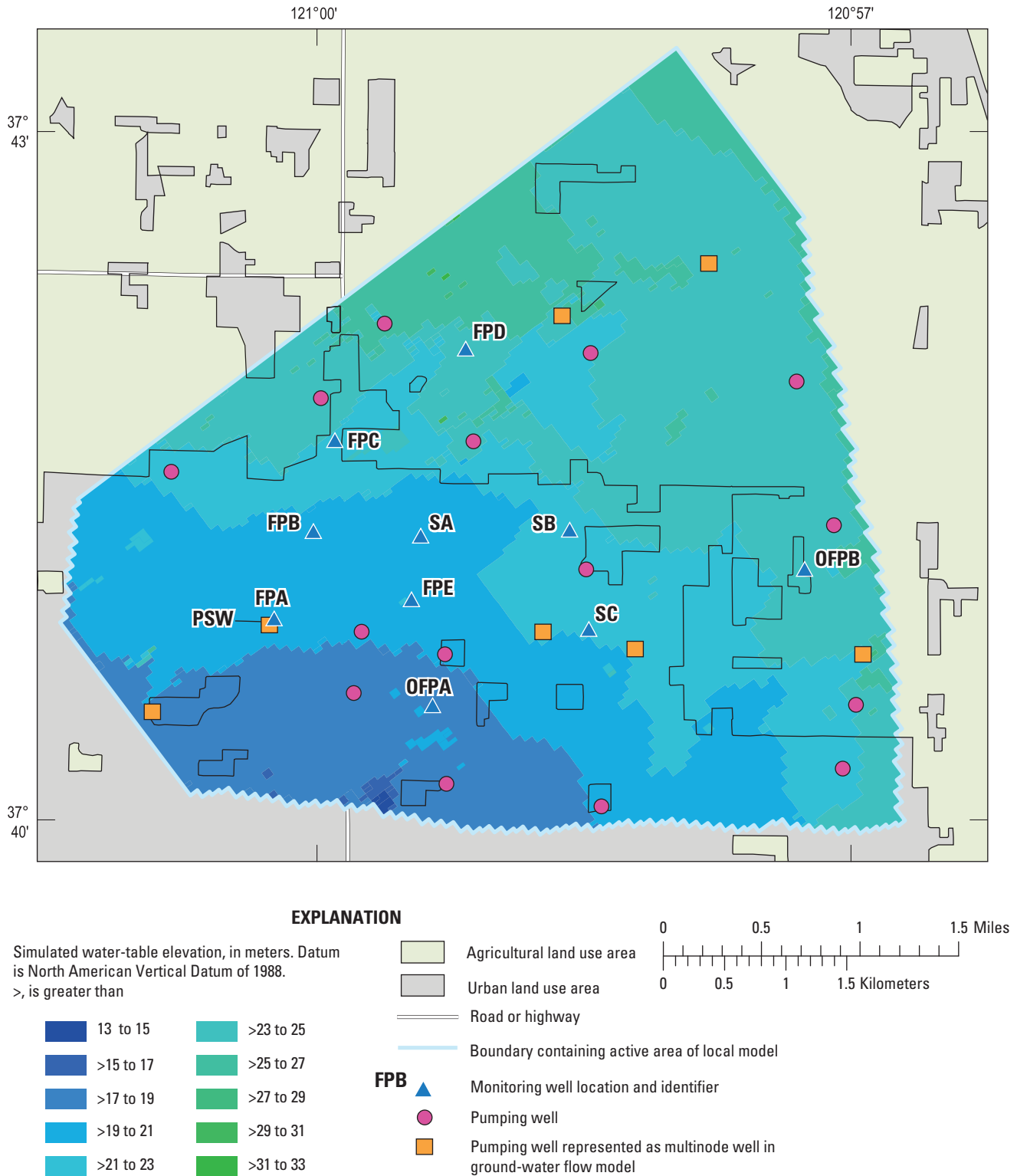


**Figure 8.** Simulated water table elevation in local ground-water flow model near Modesto, eastern San Joaquin Valley, California. PSW, public-supply well.

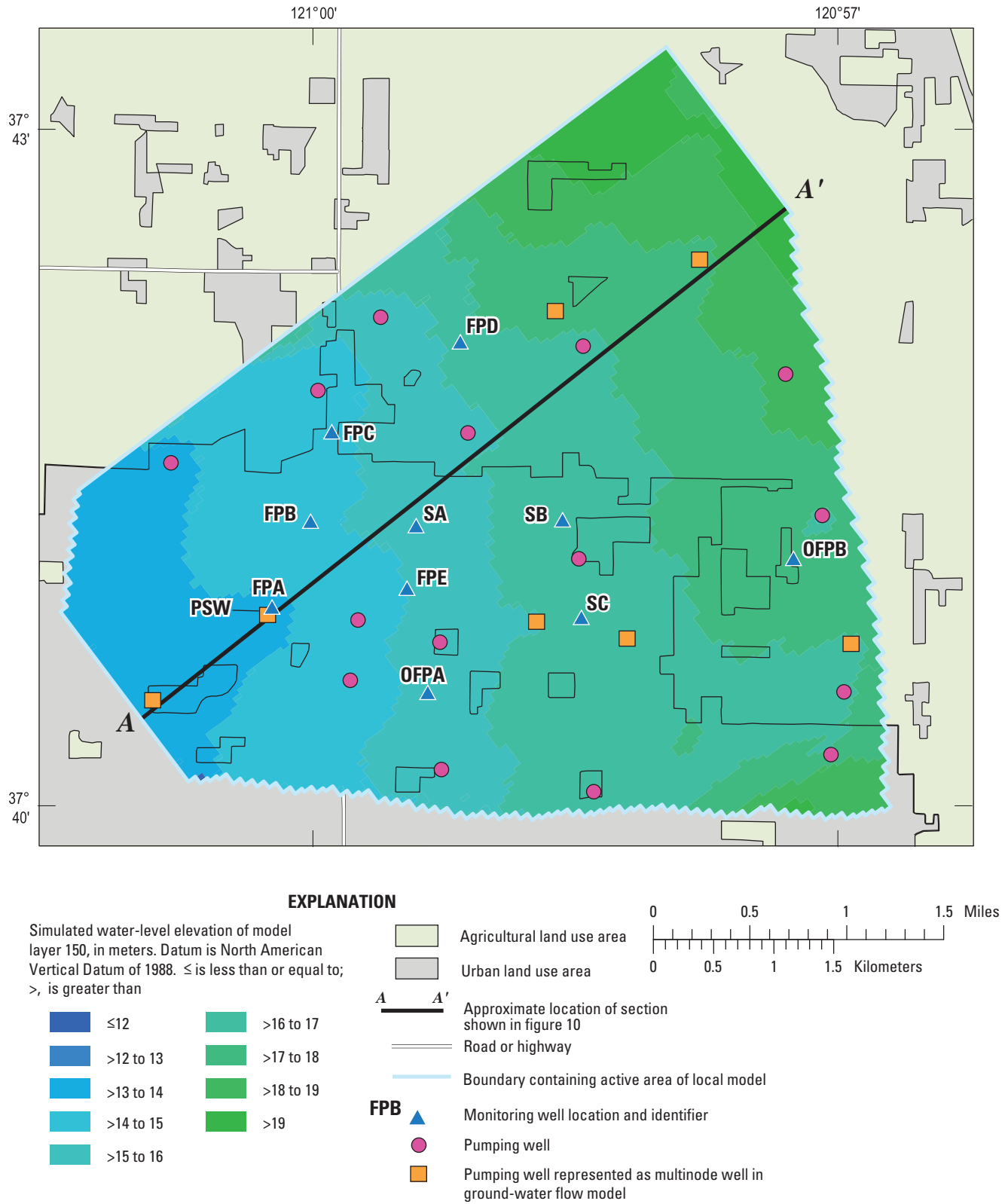


**Figure 9.** Simulated water level in model layer 150 in local ground-water flow model near Modesto, eastern San Joaquin Valley, California. PSW, public-supply well.

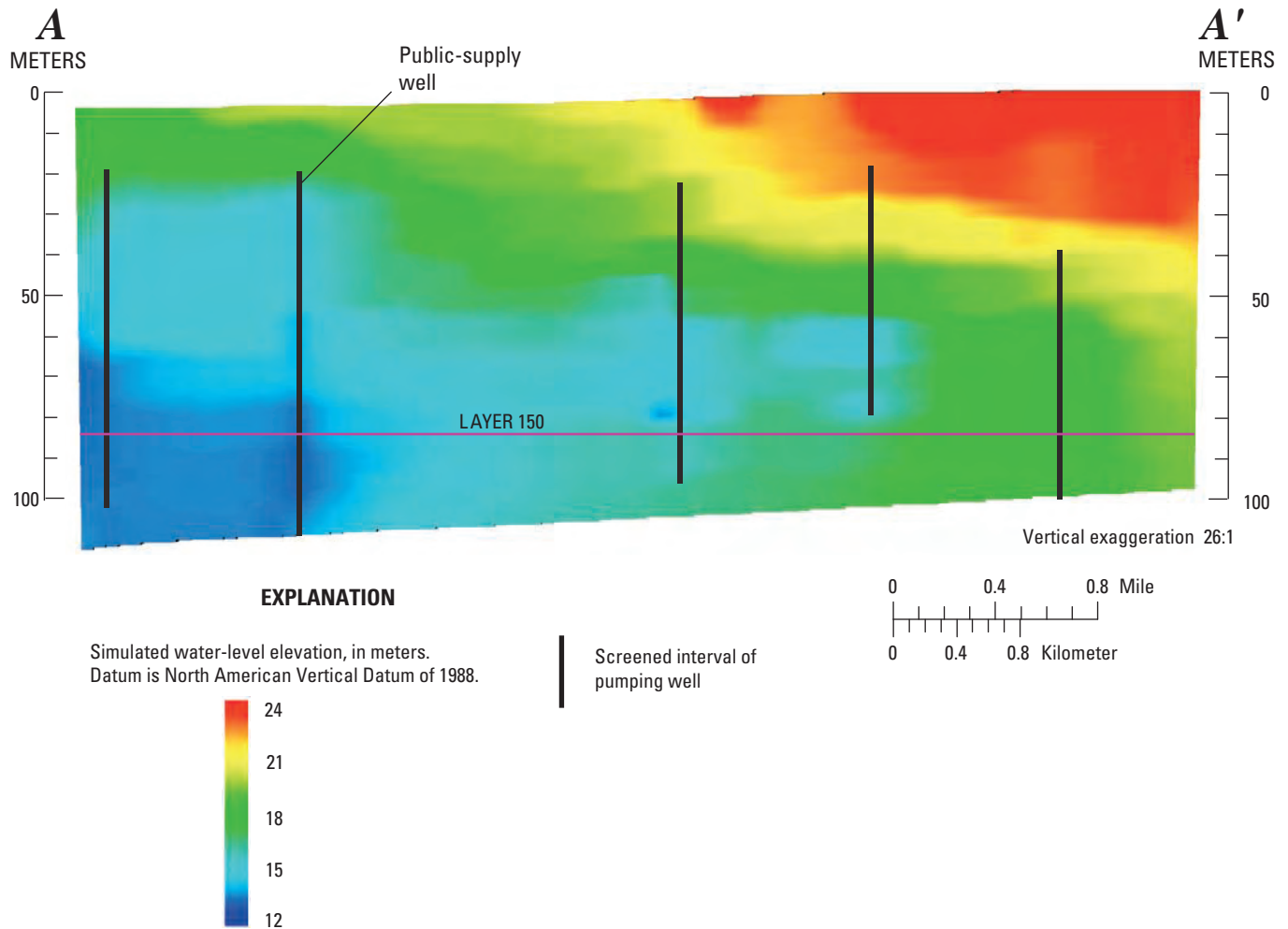


**Figure 10.** Simulated water level along vertical transect A-A' in local ground-water flow model near Modesto, eastern San Joaquin Valley, California. Location of transect shown on figure 9.

**Table 4.** Volumetric budget of local ground-water flow model near Modesto, eastern San Joaquin Valley, California.

| Boundary or stress  | In                      | Out    |
|---------------------|-------------------------|--------|
|                     | In cubic meters per day |        |
| Constant head       | 63,381                  | 39,989 |
| Recharge            | 25,091                  | 0      |
| Specified flows     | 9,220                   | 7,948  |
| Wells               | 381                     | 50,327 |
| Total               | 98,073                  | 98,264 |
| Percent discrepancy | -0.19                   |        |

### Methods and Model Parameters

Ground-water pathlines and advective travel times for the calibrated local ground-water flow model were calculated using the program MODPATH (Pollock, 1994). The travel times calculated using this method represent an average travel time for the advection of a “particle” of water or conservative solute, but also includes the effects of macro-scale mechanical dispersion caused by the three-dimensional distribution of hydrofacies.

An effective porosity was specified for each active cell according to the hydrofacies category defined for that cell. An effective porosity of 0.20 was used for the gravel hydrofacies; 0.25 was used for the sand hydrofacies; 0.30 was used for the muddy sand hydrofacies; 0.35 was used for the mud hydrofacies. Effective porosities were estimated at the low end of a range of total porosity values (Domenico and Schwartz, 1998); the weighted-average effective porosity was 31 percent.



Simulated tracer concentrations in the public-supply well were computed using forward tracking from recharge areas to the screened interval of the public-supply well. The particles were uniformly distributed on the face of the model cells associated with the inflow to the model. The flow associated with each particle was computed by dividing the inflow at the source face by the number of particles started at that face. The subset of particles that terminated at the public-supply well was used to define the area contributing recharge to that well. The flow and travel times associated with those particles that discharged at the public-supply well were then used to estimate tracer concentrations. The tracer concentration was assigned to each particle on the basis of the travel time and by assuming an input concentration of the tracer over time. A flux-weighted average concentration for the public-supply well was determined by multiplying the sum of the concentrations of particles in each layer by the total flow associated with that layer, and summing all the layers. Some particles that reached the public-supply well did not originate at recharge cells in the local model; rather, they originated at the lateral boundaries of the local ground-water flow model. In these cases, particles were placed at recharge locations in the regional ground-water flow model and tracked to equivalent locations on the lateral boundary of the regional model. The resulting travel times for these particles are the sum of the travel times from the local and the regional ground-water flow models. These particles, which did not originate at the recharge boundary in the local model, accounted for less than 0.5 percent of the flow to the well.

Simulated ages and CRAs also were computed for 23 monitoring wells sampled in this study by backtracking particles from each well screen to their recharge area. Similar to the particle tracking for the public-supply well, some particles did not terminate at recharge cells but instead terminated at the lateral boundaries of the local model. Particles were placed at equivalent locations along the lateral boundary of the regional ground-water flow model and tracked backwards to recharge locations.

## Particle Tracking Results and Comparison to Age Tracer Concentrations

The CRA and ZOC were computed for the public-supply well and the monitoring wells in the study area to evaluate particle travel times (hereinafter referred to as simulated age), and to relate ground-water quality to land use in the CRA. The computed CRA for the public-supply well covers about 45 km<sup>2</sup> and extends from about 0.5 km to the south and southwest of the well to about 2 km to the north and northeast of the well (fig. 11), overlying both the urban and the agricultural areas. The age of particles recharged in different cells varies spatially within the CRA, influenced by the heterogeneous hydrofacies distribution used in the model. In general, particle ages are less than about 30 years immediately northeast of the well and in the northwestern part of the CRA,

whereas ages exceed 90 years southeast of the well and on the northeastern edge of the CRA. Although the simulated CRA does not exactly represent the recharge area and age of ground water reaching the public-supply well, the ‘patchy’ appearance of recharge areas of young age adjacent to recharge areas of old age is probably a realistic feature of this aquifer system and is consistent with the conceptual understanding of the hydrogeology.

The simulated ages of particles reaching the public-supply well ranged from 9 to 30,000 years; the median was 54 years (table 5). Particle ages were weighted according to the flow associated with each particle for each layer along the well screen. Simulated ages indicate that a large proportion of the water contributed to the public-supply well is less than about 75 years old (fig. 12); however, 25 percent of the water is more than 100 years old, indicating that the well pumps water of a mixture of ages, spanning a wide range of hydraulic conditions in the aquifer system over time.

The age of the ground water contributed to the public-supply well increases with depth below the water table (fig. 13), reflecting a generally linear increase in age with depth in the shallow part of the well (less than 45 m below the water table) and a logarithmic increase in age with depth in the deeper part of the well. At depths of less than about 45 m below the water table, particle ages are less than 100 years. At depths of more than 60 m below the water table, the particle ages range from 140 to 1,300 years, constituting 25 percent of the flow to the well. The maximum weighted particle age of more than 30,000 years was calculated to be 75 m below the water table (not shown on figure 13). Flow to the well at this depth represents only 0.8 percent of the total flow to the well because of the fine-grained layers adjacent to the screen, which is consistent with a lack of measured wellbore flow in this interval during pumping (Jurgens and others, in press). Because the public-supply well did not exist 140 years ago and the intensity of pumping in the ground-water system did not increase until the 1940s or 1950s, the steady-state pumping conditions represented in the model likely represent a minimum age of ground water at depths more than 60 m below the water table. Prior to pumping, travel times to the deep part of the aquifer were likely much longer. Ground water entering the bottom of the well more than 60 m below the water table was expected to be generally unaffected by anthropogenic inputs at the land surface.

The simulated ages of particles reaching the 23 monitoring wells were similar to the simulated ages of particles reaching the public-supply well at similar depths in the aquifer (fig. 13). The median simulated age of particles reaching water table wells ranged from 0.4 to 7.3 years, and the median simulated age of particles reaching intermediate-depth wells ranged from 31 to 150 years. The median simulated age of particles reaching the deepest monitoring wells at depths equal to the deepest part of the public-supply well ranged from 1,100 to 1,700 years (table 6).



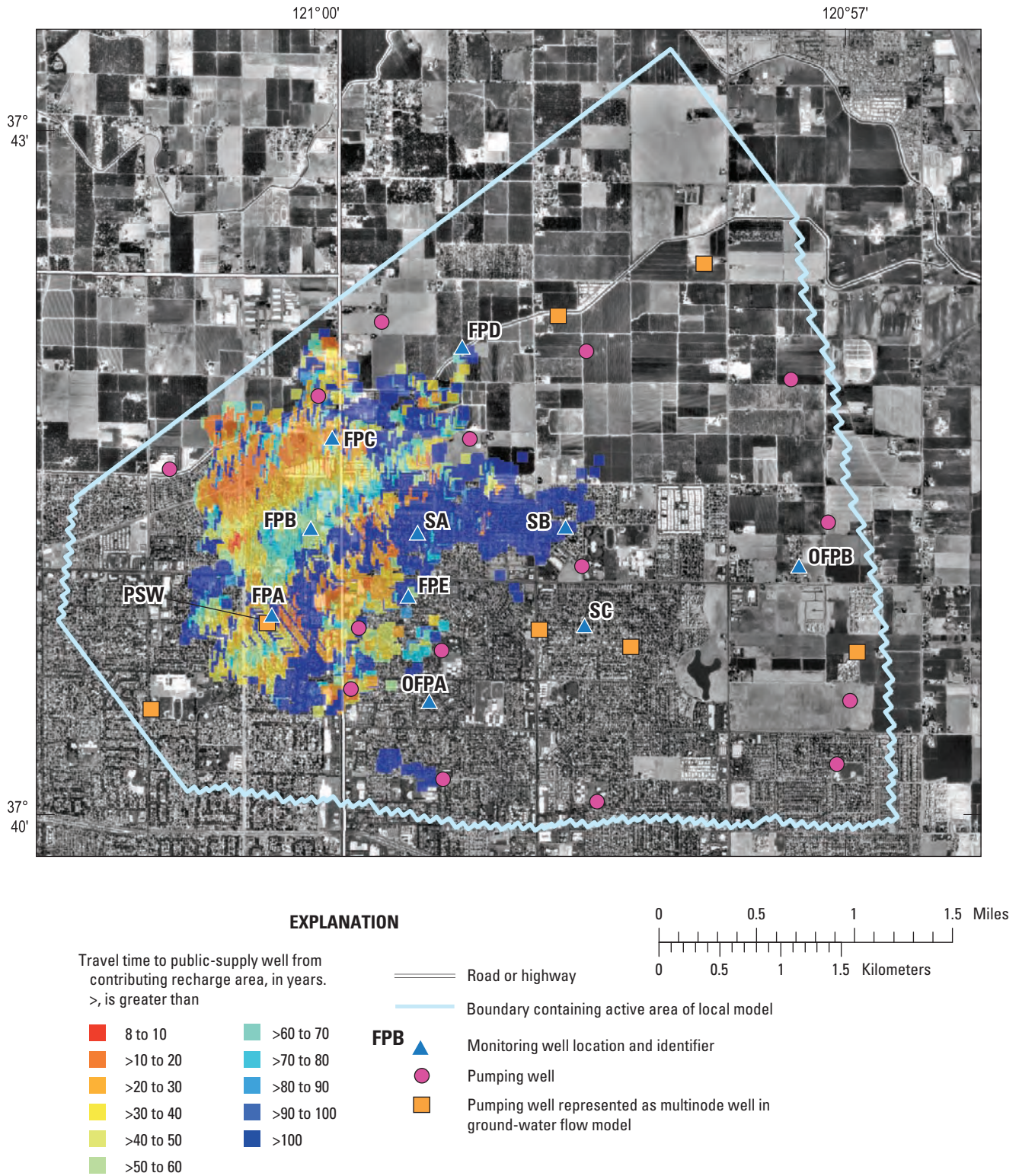


**Figure 11.** Contributing recharge area and particle travel times to public-supply well near Modesto, eastern San Joaquin Valley, California. PSW, public-supply well.

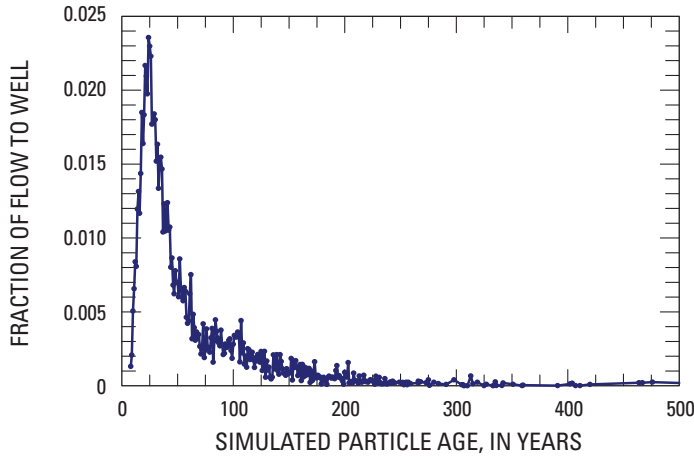


**Figure 12.** Simulated flow-weighted age of particles reaching the public-supply well near Modesto, eastern San Joaquin Valley, California.

Ground-water ages derived by interpreting samples of age dating tracers (Jurgens and others, in press) generally agree with simulated ages (tables 5 and 6; fig. 13). The median simulated age of 54 years for water in the public-supply well is similar to the interpreted age of 55 years from age-dating tracers; however, the interpreted ages were more than 50 percent older than the median simulated ages for water in 2 water table wells (FPC-1 and FPD-1), 1 intermediate-depth well (FPD-2), and all 4 deep wells (FPA-4, FPB-3, FPC-3, and FPD-3). Simulated ages in the deep monitoring wells should differ from interpreted ground-water ages from the age-dating tracers because steady-state conditions that included pumping were simulated and the oldest interpreted ages pre-date pumping. The simulated age was older than the age interpreted from age-dating tracers only in the public-supply well and in monitoring well FPB-2.

The ground-water age interpreted from age-dating tracers is not measured directly. Interpreted ground-water age is estimated using simple analytical models that describe age distributions for various combinations of recharge area and aquifer geometry (Cook and Böhlke, 1999). Although the comparison between simulated and interpreted ground-water ages is useful to generally evaluate whether simulated ages reasonably represent measured ages, direct comparison is difficult. The age interpreted from age-dating tracers does not directly account for the age and fraction of pre-tracer-aged water in the sample, and some simplifying assumptions about the age distribution of the flow system must be made in the interpretation.

A more robust comparison between simulated ground-water age and interpreted age from age-dating tracers was made by comparing simulated and measured concentrations of the age-dating tracers rather than simulated and interpreted ages. Concentrations were assigned to particles on the basis of flow-weighted particle age and input concentration histories for sulfur hexafluoride (SF<sub>6</sub>) and tritium (<sup>3</sup>H) (fig. 14). Atmospheric concentrations of SF<sub>6</sub> have increased since the 1950s, and SF<sub>6</sub> concentrations have been used to date recently recharged ground water (Busenberg and Plummer, 2000; Böhlke, 2005). Concentrations of <sup>3</sup>H in precipitation (Michel, 1989) peaked in the 1960s (fig. 14), indicating that the comparison to concentrations between simulated and measured <sup>3</sup>H concentrations could be non-unique. <sup>3</sup>H concentrations were adjusted for radioactive decay to 2004 assuming a 12.3 year half-life. Ground-water samples were collected from the public-supply well and shallow monitoring wells, and were analyzed for dissolved SF<sub>6</sub> gas and <sup>3</sup>H concentrations (Jurgens and others, in press); concentrations measured in the wells were compared with simulated concentrations.

**Table 5.** Summary statistics for the simulated contributing recharge area and the zone of contribution of the public-supply well near Modesto, eastern San Joaquin Valley, California.

[ZOC, zone of contribution. m, meter; km<sup>2</sup>, square kilometer; m/d, meter per day; m<sup>3</sup>, cubic meter; m<sup>3</sup>/d, cubic meter per day]

|  |                              |
|--|------------------------------|
| Depth to top of screened interval                                  | 27.7                         |
| Depth to bottom of open interval                                   | (m below land surface) 119.2 |
| Depth to water   | 10.2                         |
| Ground-water age interpreted from age tracers (years) <sup>1</sup> | 55                           |
| Simulated ground-water age (years) <sup>2</sup>                    |                              |
| Minimum  | 9                            |
| Median   | 54                           |
| Mean   | 420                          |
| Maximum  | 30,000                       |
| Area contributing recharge (km <sup>2</sup> )                      | 45                           |
| Mean velocity (m/d)  | 0.026                        |
| Median velocity (m/d)  | 0.017                        |
| Volume of ZOC (m <sup>3</sup> )                                    | 325,000,000                  |
| Pumping rate (m <sup>3</sup> /d)                                   | 3,746                        |

<sup>1</sup>Interpreted ground-water age is from Jurgens and others (in press).

<sup>2</sup>Simulated ground-water age for public-supply well is flow-weighted average of particle travel times for each model layer at well screen.



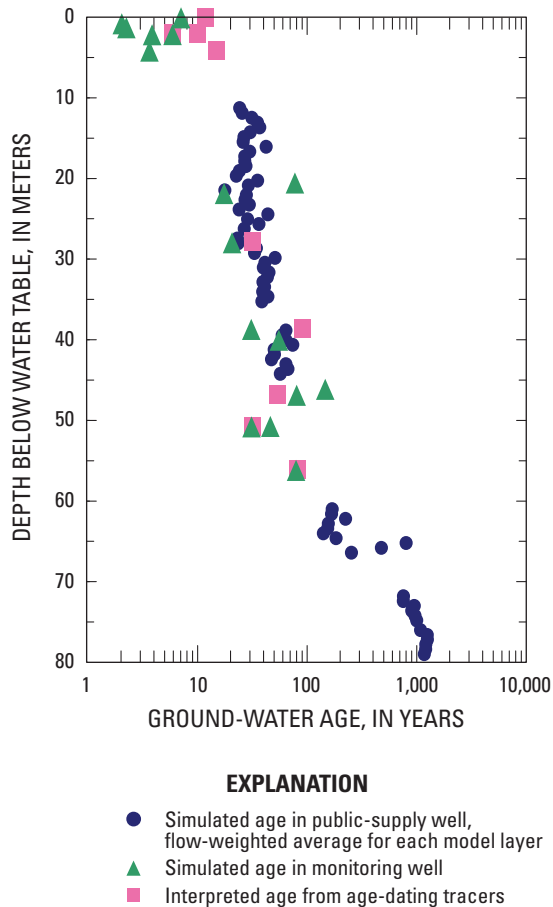


**Figure 13.** Simulated age and interpreted ground-water age from age-dating tracers, as compared with depth below water table in monitoring wells and the public-supply well near Modesto, eastern San Joaquin Valley, California. Simulated ages in the public-supply well are flow-weighted. Interpreted ground-water age from Jurgens and others, in press.

The simulated  $\text{SF}_6$  concentration of 0.40 part per trillion by volume (pptv) in the public-supply well was lower than the measured concentration of 0.73 pptv (fig. 15A). Similarly, simulated concentrations of  $\text{SF}_6$  for the monitoring wells were lower than measured concentrations in the intermediate-depth monitoring wells (FPB-2, FPC-2, FPD-2) and higher than measured concentrations in the water table wells, especially in wells FPC-1 and FPD-1. Although simulated concentrations were not expected to exactly match measured concentrations because the hydraulic conductivity distribution did not reflect the true distribution, Jurgens and others (in press) noted that  $\text{SF}_6$  concentrations measured in shallow ground water were lower than expected, and measured concentrations in intermediate-depth ground water were higher than expected, for ages interpreted from other ground-water age tracers.

The simulated  $^3\text{H}$  concentration of 5.8 tritium units (TU) in the public-supply well was slightly higher than the measured concentration of 4.6 TU (fig. 15B). Many of the simulated concentrations of  $^3\text{H}$  for the monitoring wells were similar to measured concentrations; however, simulated concentrations were much lower than measured concentrations in 6 wells (FPA-2, FPA-3, FPB-2, FPE-2, OFPA-2, and OFPB-2) and much higher than measured concentrations in 1 well (FPD-2). All of these wells are screened in the intermediate depths in the aquifer. The reasons for concentrations being lower could be because of possible differences in measured and calibrated hydraulic conductivity values (at each well), although results for only 3 of the 6 wells could be explained by differences in hydraulic conductivity. Also, simulated concentrations of  $^3\text{H}$  at intermediate depths are strongly sensitive to the particle ages because  $^3\text{H}$  concentrations peak (fig. 14) during the recharge dates of water contained in this zone. Overall, the trend for simulated  $^3\text{H}$  concentrations with depth in both the public-supply well and the monitoring wells generally corresponds with the trend in measured  $^3\text{H}$  concentrations with depth (fig. 16).

### Comparison between Land Use in the Contributing Recharge Area (CRA) and Occurrence of Selected Constituents

The local ground-water flow model generally matches observed conditions in the ZOC of the public-supply well, and can be used to link sources of contaminants in the CRA with concentrations in the public-supply well. The CRA for the public-supply well lies predominantly beneath the current (2001) urban land use area (fig. 11). Analysis of recent land-use maps indicates that about 67 percent of the CRA is beneath urban land, whereas only 32 percent is beneath agricultural land (table 7). Both agricultural and urban contaminants are expected to exist at the water table beneath the CRA. The urban area has expanded north and west of the public-supply well since the 1960s, with residential and commercial development replacing agricultural land.

Ground water within the ZOC older than about 40 years was expected to contain primarily agricultural-related contaminants, whereas ground water younger than 40 years was expected to contain both urban and agricultural contaminants. Elevated concentrations of nitrate and low concentrations of VOCs and pesticides have been measured in the public-supply well (table 7), which is consistent with both agricultural and urban sources. Although elevated concentrations of nitrate do not indicate exclusively agricultural input, previous monitoring of ground-water quality beneath agricultural land (Burow and others, 1998; Burow and others, in press) has increased expectations of elevated nitrate levels.

**Table 6.** Well characteristics and simulated and interpreted ground-water ages from age-dating tracers in monitoring wells sampled in 2003-2005 near Modesto, eastern San Joaquin Valley, California.

[—, no data]

| Well name                     | Depth category/ Well type <sup>1</sup> | Depth to top of screened interval | Depth to bottom of screened or open interval | Depth to water | Ground-water age interpreted from age tracers <sup>2</sup> (years) | Simulated ground-water age (years) |        |         |
|-------------------------------|--|-----------------------------------|--|----------------|--|------------------------------------|--------|---------|
|                               |  |                                   |  |                |  | Minimum                            | Median | Maximum |
| In meters below land surface) |  |                                   |  |                |  |                                    |        |         |
| FPA-1                         | Water table                            | 9.1                               | 10.7   | 7.8            | 6  | 3.3                                | 4.0    | 4.6     |
| FPA-2                         | Shallow                                | 35.1                              | 36.6   | 7.9            | 32   | 19                                 | 21     | 44      |
| FPA-3                         | Intermediate                           | 65.5                              | 67.1   | 10.1           | 81   | 74                                 | 80     | 86      |
| FPA-4                         | Deep                                   | 104.5                             | 106.1  | 10.5           | 4,600  | 1,100                              | 1,100  | 1,100   |
| FPB-1                         | Water table                            | 9.1                               | 10.7   | 7.8            | 10   | 4.8                                | 6.1    | 7.4     |
| FPB-2                         | Intermediate                           | 57.0                              | 58.5   | 10.9           | 53   | 59                                 | 80     | 100     |
| FPB-3                         | Deep                                   | 100.0                             | 101.5  | 11.5           | 9,300  | 1,300                              | 1,400  | 1,500   |
| FPC-1                         | Water table                            | 11.9                              | 13.4   | 8.5            | 15   | 3.2                                | 3.8    | 4.3     |
| FPC-2                         | Intermediate                           | 61.9                              | 63.4   | 11.8           | 32   | 32                                 | 32     | 32      |
| FPC-3                         | Deep                                   | 105.8                             | 107.3  | 12.2           | 8,300  | 1,600                              | 1,700  | 1,800   |
| FPD-1                         | Water table                            | 8.5                               | 10.1   | 9.3            | 12   | 0.3                                | 0.6    | 1.0     |
| FPD-2                         | Intermediate                           | 50.9                              | 52.4   | 13.0           | 90   | 31                                 | 31     | 32      |
| FPD-3                         | Deep                                   | 101.8                             | 103.3  | 13.5           | 7,100  | 1,200                              | 1,200  | 1,200   |
| FPE-1                         | Water table                            | 9.1                               | 10.7   | 8.8            | —  | 0.8                                | 0.9    | 2.0     |
| FPE-2                         | Shallow                                | 29.9                              | 31.4   | 8.8            | —  | 15                                 | 18     | 28      |
| FPE-3                         | Intermediate                           | 61.9                              | 63.4   | 11.9           | —  | 45                                 | 47     | 48      |
| OFPA-1                        | Water table                            | 9.1                               | 10.7   | 9.2            | —  | 2.1                                | 2.1    | 2.7     |
| OFPA-2                        | Shallow                                | 29.0                              | 30.5   | 9.2            | —  | 72                                 | 78     | 90      |
| OFPA-3                        | Intermediate                           | 57.3                              | 58.8   | 11.9           | —  | 140                                | 150    | 180     |
| OFPB-2                        | Intermediate                           | 50.6                              | 52.1   | 11.3           | —  | 36                                 | 56     | 64      |
| SA                            | Water table                            | 9.1                               | 10.7   | 8.7            | —  | 1.9                                | 2.3    | 12      |
| SB                            | Water table                            | 9.1                               | 10.7   | 9.3            | —  | 0.2                                | 0.4    | 0.7     |
| SC                            | Water table                            | 9.1                               | 10.7   | 10.2           | —  | 5.1                                | 7.3    | 9.5     |

<sup>1</sup>Well depth zones are depth below land surface and were characterized by Jurgens and others (in press) for use in interpreting the geochemical data.

<sup>2</sup>Interpreted ground-water ages are from Jurgens and others (in press).

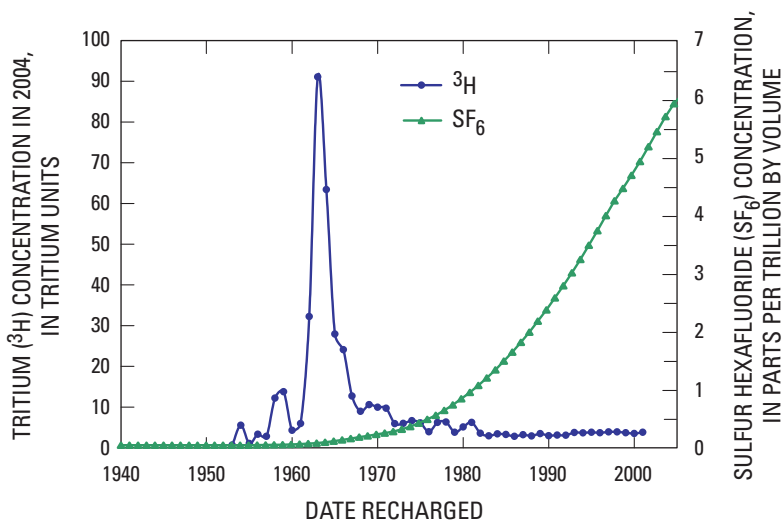


**Figure 14.** Concentrations of tritium (<sup>3</sup>H) and sulfur hexafluoride (SF<sub>6</sub>) in recharge.

<sup>3</sup>H concentrations are updated from Michel (1989) and corrected for decay to 2004; SF<sub>6</sub> concentrations are updated from Busenberg and Plummer (2000).

The stable isotope composition of ground water from the public-supply well also is consistent with the composition of surface water used for irrigation (Jurgens and others, in press), further indicating that the nitrate concentration in the public-supply well may be derived primarily from previous agricultural inputs. However, the composition of ground water reaching the public-supply well reflects urban inputs also. The VOCs detected in the public-supply well (chlorinated solvents, disinfection byproducts; Jurgens and others, in press) are likely derived from urban land-use practices because they were not detected in the agricultural monitoring networks and are typically detected in ground water beneath urban areas nationwide (Squillace and others, 2004). The pesticides detected in the public-supply well (simazine, atrazine, and desethyl atrazine) could be derived from either agricultural or urban use.

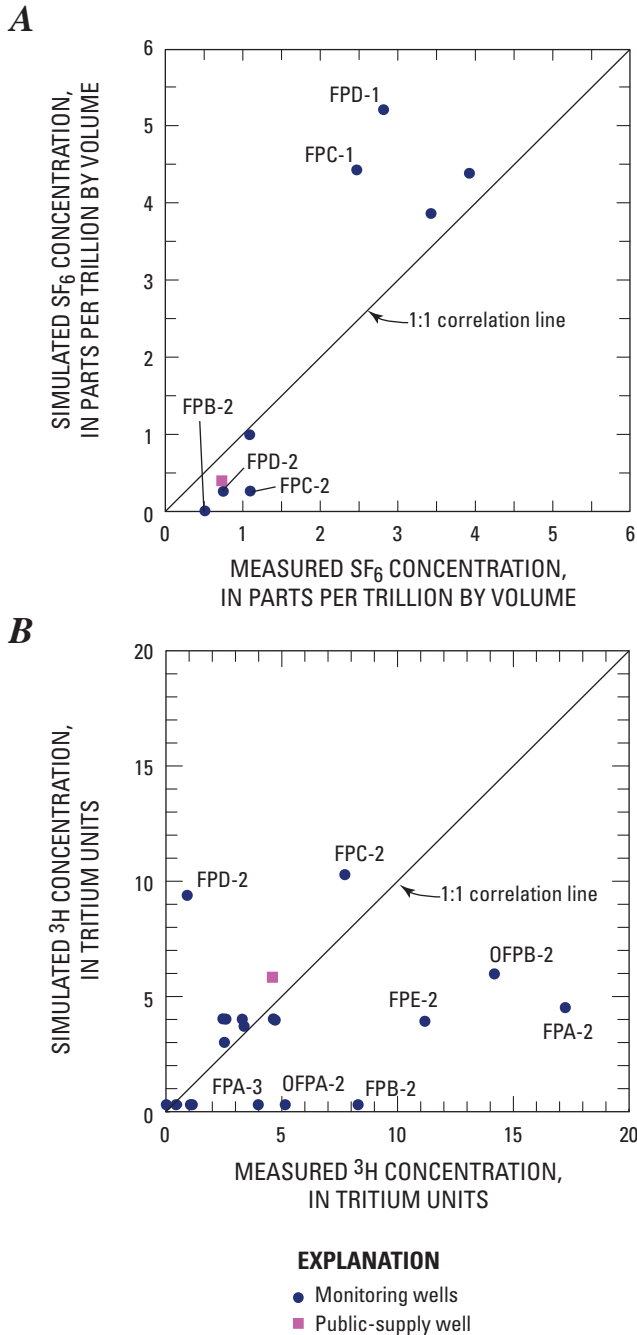


**Figure 15.** Simulated and measured concentrations of (A) sulfur hexafluoride ( $SF_6$ ) and (B) tritium ( $^3H$ ) in monitoring wells and the public-supply well near Modesto, eastern San Joaquin Valley, California.

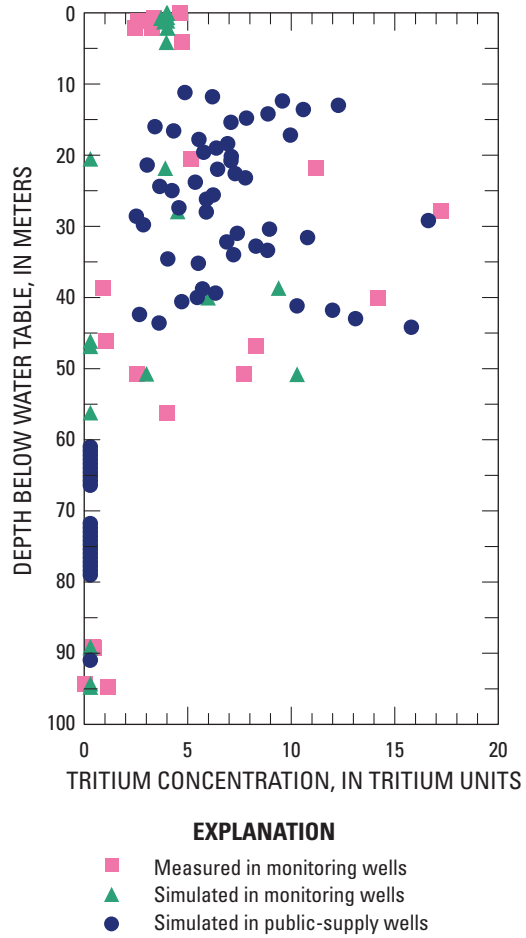


**Figure 16.** Simulated and measured tritium ( $^3H$ ) concentrations with depth in monitoring wells and the public-supply well near Modesto, eastern San Joaquin Valley, California.

Land use in the CRAs for the monitoring wells in the study area ranged from 100 percent urban land to 100 percent agricultural land; two wells were each in a CRA that had a mixture of urban and agricultural land use (FPA-2 and SA) (table 7). Most of the wells with CRAs containing 100 percent agricultural land use had concentrations of nitrate that were consistent with either agricultural or old, unaffected groundwater. Three wells, FPA-4, FPC-2, and OFPB-2, had VOCs typically found in urban land-use settings, in spite of having a CRA containing 100-percent agricultural land use. FPA-4 was affected by downward movement of contaminants through the adjacent public-supply well when the public-supply well was not in operation (Jurgens and others, in press). Both FPC-2 and OFPB-2 are in areas in transition from agricultural to urban land use, and might be influenced by newer urban development.

**Table 7.** Nitrate concentrations, volatile organic compound and pesticide occurrence, and relation to land use in the contributing recharge areas of the public-supply well and monitoring wells in Modesto, eastern San Joaquin Valley, California.

[The land-use data set used for these classifications was an enhanced version of the U.S. Geological Survey 1992 National Land Cover Data (NLCD), which classified land use by each 30- by 20-meter area of land in the conterminous United States; the original and enhanced versions of the NLCD are described by Vogelmann and others (2001) and Nakagaki and Wolock (2005), respectively. Nitrate, VOC, and pesticide data are reported by Jurgens and others (in press). mg/L, milligrams per liter; N, nitrogen; —, no data; VOC, volatile organic compound, PSW, public-supply well]

| Well name | Nitrate concentration (mg/L, as N) | Number of VOCs detected | Number of pesticides detected <sup>1</sup> | Median age of simulated groundwater (years) | Recent general land use in contributing recharge area |              | Recent detailed land use in contributing recharge area |                           |   |   |                        |                          |                                   |           |
|-----------|------------------------------------|-------------------------|--|---|---|--------------|--|---------------------------|---|---|------------------------|--------------------------|-----------------------------------|-----------|
|           |                                    |                         |  |   | Urban   | Agricultural | Urban: Low intensity residential                       | Urban: Residential/ other | Urban: Commercial/ industrial/ transportation | Agriculture: Orchards/ vineyards/ other | Agriculture: Row crops | Agriculture: Pasture/hay | Rangeland: Grasslands/ herbaceous |           |
|           |                                    |                         |  |   |   |              |  |                           |   |   |                        |                          |                                   | (percent) |
| PSW       | 5.5                                | 5                       | 3  | 54  | 67  | 30           | 50   | 4                         | 13  | 4                                       | 4                      | 4                        | 22                                | 2         |
| FPA-1     | 1.5                                | 3                       | 4 (URB)                                    | 4.0   | 100   | 0            | 100  |                           |   |   |                        |                          |                                   |           |
| FPA-2     | 12                                 | 2                       | 0  | 21  | 52  | 48           | 17   | 18                        | 17  | 40                                      |                        |                          | 8                                 |           |
| FPA-3     | 3.0                                | 0                       | 0  | 80  | 0   | 100          |  |                           |   | 100                                     |                        |                          |                                   |           |
| FPA-4     | 2.4                                | 2                       | 1  | 1,100                                       | 0   | 100          |  |                           |   |   |                        |                          | 100                               |           |
| FPB-1     | 3.2                                | 3                       | 0  | 6.1   | 100   | 0            | 100  |                           |   |   |                        |                          |                                   |           |
| FPB-2     | 4.0                                | 1                       | 0  | 80  | 100   | 0            | 4  | 34                        | 62  |   |                        | 92                       | 8                                 |           |
| FPB-3     | 1.0                                | 0                       | 0  | 1,400                                       | 0   | 100          |  |                           |   |   |                        |                          |                                   |           |
| FPC-1     | 13                                 | 4                       | 4  | 3.8   | 100   | 0            | 100  |                           |   |   |                        |                          |                                   |           |
| FPC-2     | 8.7                                | 1                       | 2 (AG)                                     | 32  | 0   | 100          |  |                           |   | 100                                     |                        |                          |                                   |           |
| FPC-3     | 1.5                                | 0                       | 0  | 1,700                                       | 0   | 100          |  |                           |   |   |                        | 100                      |                                   |           |
| FPD-1     | 17                                 | 0                       | 4 (AG)                                     | 0.6   | 0   | 100          |  |                           |   |   |                        |                          |                                   |           |
| FPD-2     | 4.0                                | 0                       | 1 (AG)                                     | 31  | 0   | 100          |  |                           |   |   |                        |                          |                                   |           |
| FPD-3     | 1.8                                | 1                       | 0  | 1,200                                       | 100   | 0            |  | 100                       |   |   |                        |                          |                                   |           |
| FPE-1     | 1.8                                | 1                       | 3 (URB)                                    | 0.9   | 100   | 0            | 100  |                           |   |   |                        |                          |                                   |           |
| FPE-2     | 13                                 | 3                       | 3  | 18  | 100   | 0            | 92   |                           |   |   | 8                      |                          |                                   |           |
| FPE-3     | 5.6                                | 0                       | 0  | 47  | 100   | 0            | 100  |                           |   |   |                        |                          |                                   |           |
| OFPA-1    | 3.1                                | 5                       | 2  | 2.1   | 100   | 0            | 64   |                           |   | 36                                      |                        |                          |                                   |           |
| OFPA-2    | 12                                 | 0                       | 0  | 78  | 100   | 0            | 83   |                           |   | 17                                      |                        |                          |                                   |           |
| OFPA-3    | 4.4                                | 0                       | 0  | 150   | 100   | 0            | 96   |                           |   | 4                                       |                        |                          |                                   |           |
| OFPB-2    | 1.6                                | 2                       | 2  | 56  | 0   | 98           |  |                           |   |   | 31                     |                          | 67                                | 2         |
| SA        | 2.4                                | 4                       | 1 (AG)                                     | 2.3   | 81  | 19           | 81   |                           |   |   |                        |                          | 19                                |           |
| SB        | 6.5                                | 3                       | 2  | 0.4   | 100   | 0            | 100  |                           |   |   |                        |                          |                                   |           |
| SC        | 11                                 | 8                       | 1  | 7.3   | 100   | 0            | 100  |                           |   |   |                        |                          |                                   |           |

<sup>1</sup>Pesticide use category in parentheses: URB, urban use only; AG, agricultural use only; no designation, pesticide is used in both urban and agricultural land-use settings.

Six of the 13 wells in a CRA where 100-percent of the land was urban had nitrate concentrations above 5 mg/L: FPC-1, FPE-2, FPE-3, OFPA-2, SB, and SC. Because many of the wells contain ground water that was recharged tens to thousands of years ago, concentrations of nitrate or other constituents may not be derived from recent land use. Therefore, the wells were also classified with respect to the most likely source of nitrate by evaluating the geochemistry of the ground water and determining the likely land use in the CRA at the time of recharge based on approximate dates of urban development (table 8). Nitrate concentrations in ground water reaching wells FPC-1, FPE-2, FPE-3 and OFPA-2 were elevated because of previous agricultural land use. However, elevated nitrate concentrations in ground water from SB and SC are likely due to septic inputs, on the basis of bromide-to-chloride ratios and the location of unsewered subdivisions (Jurgens and others, in press). The public-supply well, and 6 of the 12 wells containing nitrate derived from agricultural land use, contained VOCs also (FPA-2, FPB-2, FPC-1, FPC-2, FPE-2, and OFPB-2), suggesting that ground water from these wells could contain a mixture of urban and agricultural inputs. Most of these wells were screened at intermediate depths, from 20 to 50 m below the water table. In general, concentrations of nitrate in ground water dominated by agricultural inputs are high (median 7.2 mg/L), whereas concentrations in ground water dominated by urban inputs are low (median 3.1 mg/L) (table 8).

### Processes Affecting Nitrate and Uranium Concentrations in the Aquifer and the Public-Supply Well

Nitrate concentrations in the ZOC of the public-supply well were highest near the water table beneath the agricultural land and at the shallow depth (table 8). Concentrations were above the MCL of 10 mg/L (U.S. Environmental Protection Agency, 2006) in 2 wells screened near the water table beneath the agricultural area and in 1 well beneath the urban area. The median nitrate concentration in wells screened near the water table beneath the agricultural area was 15 mg/L, whereas the median concentration in wells screened near the water table beneath the urban area was only 3.1 mg/L. Nitrate concentrations decrease with depth to background concentrations equaling about 2 mg/L or less in the deepest wells. Most of the aquifer is oxic (Jurgens and others, in press); therefore, nitrate was expected to be transported conservatively through the system. Nitrate concentration in the public-supply well (5.5 mg/L) was between concentrations in the shallow and the deep part of the ZOC because of the mixture of zones contributing ground water to the well. Wells were divided into water table (less than 5 m below the water table), shallow (up to 50 m below land surface), and intermediate (50 to 70 m below land surface), and deep zones (greater than 70 m below land surface) on the basis of depth and geochemistry of water reaching the wells (Jurgens and

others, in press). Nitrate concentrations in the shallow depth zone are similar to concentrations at the water table beneath the agricultural area; concentrations are much lower in the intermediate depth zone (table 8). Because of the mostly downward movement of water in the study area, nitrate in shallow ground water is likely to continue moving downward.

Long-term nitrate concentrations in the public-supply well will depend on the relative proportions of urban and agricultural land within the CRA of the well and the amount of nitrogen input within each of these settings. High nitrate concentrations derived from agricultural fertilizer and low nitrate concentrations near the water table from urban recharge will continue to move downward and contribute to the total nitrate concentrations in the well. If nitrate input beneath the urban area remains low, then nitrate concentrations in the public-supply well will level off and decrease. If nitrate input beneath the agricultural area increases significantly, nitrate concentrations could increase in the public-supply well, although urban development in the CRA would decrease the amount of agriculturally-derived water reaching the well.

Fertilizers were the primary source of nitrate in the ZOC of the public-supply well. The generally high concentrations beneath the agricultural area, low concentrations beneath the urban area, and the decrease in nitrate concentrations below the shallow depth are consistent with the history of nitrogen fertilizer use. Estimates of nitrogen concentrations in recharge water from nitrogen fertilizer applied over time were used as input concentrations for the simulation of nitrate concentrations in the public-supply well (fig. 17). Nitrate concentrations in recharge water were estimated using a method outlined by Böhlke (2002) using ground-water recharge dates and county-based nitrogen fertilizer application data (Alexander and Smith, 1990; Ruddy and others, 2006). This method is described below.

On the basis of mean ground-water ages from age-dating tracers collected in the monitoring wells, a linear ground-water age gradient with depth was characterized (Cook and Böhlke, 1999), indicating a constant vertical velocity with depth for ground water younger than about 60 years. The estimated recharge rate,  $r$ , was calculated using the equation,

$$r = nZ / \tau, \quad (1)$$

where

$n$  is the effective porosity,

$Z$  is the saturated thickness of the aquifer, and

$\tau$  is the mean age of ground water in the aquifer

(Cook and Böhlke, 1999; Böhlke, 2002).

**Table 8.** Nitrate, alkalinity and uranium concentrations from monitoring wells and the public-supply well sampled in 2003–2005 near Modesto, eastern San Joaquin Valley, California.[Ag, agricultural; mg/L, milligram per liter; µg/L, microgram per liter; N, nitrogen; CaCO<sub>3</sub>, calcium carbonate; PSW, public-supply well]

| Well name                                 | Dominant land use affecting nitrate concentrations | Nitrate concentration, in mg/L as N | Uranium concentration, in µg/L | Alkalinity, dissolved (mg/L as CaCO <sub>3</sub> ) |
|---|--|-------------------------------------|--------------------------------|--|
| Water table well depth zone <sup>1</sup>  |  |                                     |                                |  |
| FPA-1                                     | Urban  | 1.5                                 | 32                             | 363  |
| FPB-1                                     | Urban  | 3.2                                 | 11                             | 308  |
| FPC-1                                     | Ag   | 13                                  | 23                             | 376  |
| FPD-1                                     | Ag   | 17                                  | 23                             | 232  |
| FPE-1                                     | Urban  | 1.8                                 | 4.8                            | 246  |
| OFPA-1                                    | Urban  | 3.1                                 | 25                             | 416  |
| SA  | Urban  | 2.4                                 | 30                             | 494  |
| SB  | Urban  | 6.5                                 | 32                             | 446  |
| SC  | Urban  | 11                                  | 29                             | 432  |
| Median                                    |  | 3.2                                 | 25                             | 376  |
| Shallow well depth zone <sup>1</sup>      |  |                                     |                                |  |
| FPA-2                                     | Ag   | 12                                  | 24                             | 309  |
| FPE-2                                     | Ag   | 13                                  | 22                             | 298  |
| OFPA-2                                    | Ag   | 12                                  | 45                             | 380  |
| Median                                    |  | 12                                  | 24                             | 309  |
| Intermediate well depth zone <sup>1</sup> |  |                                     |                                |  |
| FPA-3                                     | Ag   | 3.0                                 | 2.5                            | 104  |
| FPB-2                                     | Ag   | 4.0                                 | 6.6                            | 144  |
| FPC-2                                     | Ag   | 8.7                                 | 10                             | 187  |
| FPD-2                                     | Ag   | 4.0                                 | 3.4                            | 127  |
| FPE-3                                     | Ag   | 5.6                                 | 4.3                            | 133  |
| OFPA-3                                    | Ag   | 4.4                                 | 3.7                            | 129  |
| OFPB-2                                    | Ag   | 1.6                                 | 4.5                            | 146  |
| Median                                    |  | 4.0                                 | 4                              | 146  |
| Deep well depth zone <sup>1</sup>         |  |                                     |                                |  |
| FPA-4                                     | Old  | 2.4                                 | 1.0                            | 89   |
| FPB-3                                     | Old  | 1.0                                 | 0.3                            | 80   |
| FPC-3                                     | Old  | 1.5                                 | 0.2                            | 79   |
| FPD-3                                     | Old  | 1.8                                 | 0.6                            | 90   |
| Median                                    |  | 1.6                                 | 0.5                            | 85   |
| Public-supply well                        |  |                                     |                                |  |
| PSW                                       | MIXED  | 5.5                                 | 11                             | 174  |

<sup>1</sup>Well depth zones are depth below land surface and were characterized by Jurgens and others (in press) for use in interpreting the geochemical data.

An effective porosity of 0.3 and a saturated thickness of 55 m were assumed. A mean ground-water age of 42 years was calculated by averaging the mean ages derived from the age-dating tracers. The resulting estimated recharge rate was 0.4 m/yr. The nitrogen application was estimated by dividing the reported nitrogen fertilizer application for the county (Ruddy and others, 2006) by the area of fertilized land in that county and assuming that 50 percent of the nitrogen fertilizer reached the water table. Similar leaching fractions have been reported for agricultural recharge in other areas in the United States (Böhlke and Denver, 1995; Böhlke, 2002). Estimated nitrate concentrations in recharge within the CRA of the public-supply well were then calculated by assuming that the proportion of agricultural input in the CRA had decreased and

the proportion of urban input had increased beginning in about 1960, when urban development began in this area. The nitrate input in the urban area was assumed to be 3.1 mg/L, which is the median concentration in water table wells beneath the urban area (table 8). The median of expected concentrations in recharge caused by nonfarm fertilizer applications during 1987–2001 (Ruddy and others, 2006) was 3.6 mg/L, which is consistent with the median concentrations measured in water table wells beneath the urban area.

The concentration of nitrate in recharge consistently increased in the agricultural area between the 1940s and 1970s (fig. 17). The axes representing nitrate concentration and nitrogen fertilizer application in figure 17 are quantitatively related through the recharge rate, such that the application



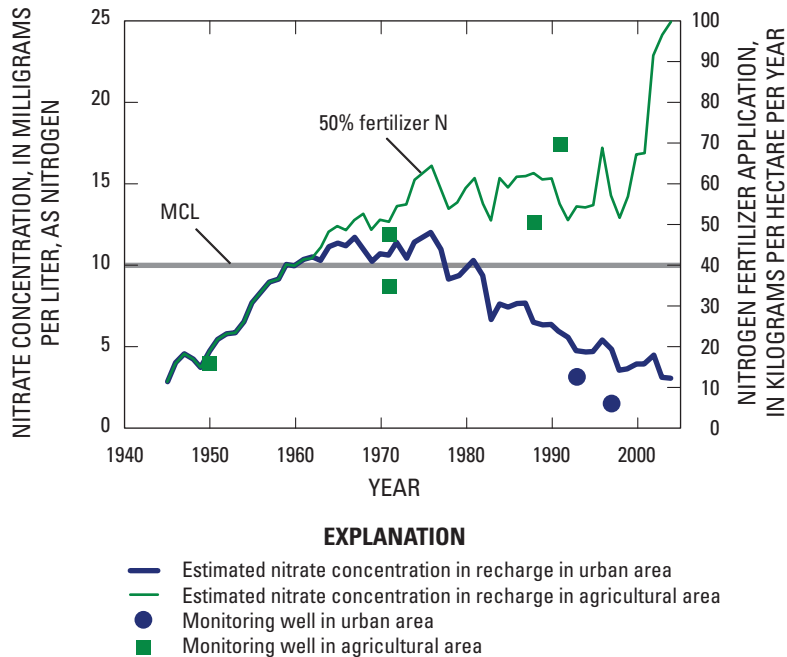


**Figure 17.** Estimated concentrations of nitrate in recharge from nitrogen fertilizer applications over time and measured nitrate concentrations in monitoring wells.

Measured concentrations of nitrate from ground water sampled during 2003–2005 are plotted against corresponding interpreted ages from age-dating tracers. The estimated concentrations of nitrate from fertilizer applications represents 50 percent of the nitrogen fertilizer applications divided by the area of fertilized land, dissolved in 0.4 meter per year of recharge. MCL, maximum contaminant level; % percent. Figure modified from Burow and others (in press).

amount on one axis corresponds to the expected concentration in recharge on the other axis. Estimated concentrations in recharge are similar to measured concentrations, although there are only 5 wells containing agriculturally-derived nitrate with corresponding ground-water recharge dates. A correlation between measured concentrations and estimated nitrate concentrations in recharge water from nitrogen fertilizer applications has been noted in other parts of the eastern San Joaquin Valley (Burow and others, 2007; Burow and others, in press). The low measured nitrate concentrations in the younger (1990s) water were from wells screened at the water table beneath the urban land-use setting and are not expected to have received agricultural fertilizer.

Results of the particle pathline analysis were used to compare simulated and measured nitrate concentrations in the public-supply well and monitoring wells. Using the same approach as that used for the  $\text{SF}_6$  and  $^3\text{H}$  comparisons, nitrate concentrations were assigned to particles on the basis of flow-weighted particle age and assuming an input concentration history for the agricultural and urban settings (fig. 17). Simulated nitrate concentrations were significantly correlated to measured nitrate concentrations in monitoring wells and

to concentrations derived from historical data from regulatory compliance monitoring records for the public-supply well ( $p = 0.002$ ,  $\rho = 0.47$ ; Spearman's rank correlation) (fig. 18). The simulated concentration of nitrate in the public-supply well was 6.0 mg/L, which is slightly higher than the measured concentration of 5.5 mg/L. Simulated concentrations in some monitoring wells were higher than measured concentrations (for example, FPD-1, FPD-2, FPC-2), and simulated concentrations in other monitoring wells were lower than measured concentrations (for example, SB, SC, OFPA-2). Some wells showed a similar discrepancy between simulated and measured tritium concentrations (FPD-2 and OFPA-2), suggesting that the simulated age distributions for these wells may not adequately reflect the actual age distribution. The measured nitrate concentration in FPD-1 was lower than simulated, likely the result of dilution by recharge of nearby canal water (Jurgens and others, in press). Measured nitrate concentrations in SB and SC were higher than simulated concentrations, probably a result of contributions from nearby septic systems.

Other possible factors affecting measured nitrate concentrations included local variability in fertilizer management near the monitoring wells, other sources of nitrate such as manure, and the mixing of ground water of different ages in the ground-water samples. Manure was not expected to be a significant source of nitrate in the study area because of the absence of confined animal operations near the wells. The method

used to compute estimated nitrogen fertilizer applications may over-estimate nitrate concentrations because of dispersion and mixing of ages in ground-water samples (Burow and others, 2007).

Measured uranium concentrations were highest near the water table (median 25  $\mu\text{g/L}$ ), and decreased in concentration with depth (median for deepest wells, 0.5  $\mu\text{g/L}$ ) (table 8). Uranium concentrations were higher than the MCL of 30  $\mu\text{g/L}$  in 2 wells screened near the water table beneath the urban area. Uranium concentrations are similar beneath agricultural (median 23  $\mu\text{g/L}$ ) and urban (median 29  $\mu\text{g/L}$ ) areas. Uranium concentrations in the shallow depth zone are similar to concentrations at the water table. Uranium concentrations have been mobilized, and high concentrations near the water table have migrated to shallow depths along with nitrate. Concentrations are much lower in the intermediate depth zone than the shallow depth zone (table 8). Uranium concentration in the public-supply well (11  $\mu\text{g/L}$ ) was between those in the shallow and the deeper part of the system because of the mixture of zones contributing to the well.

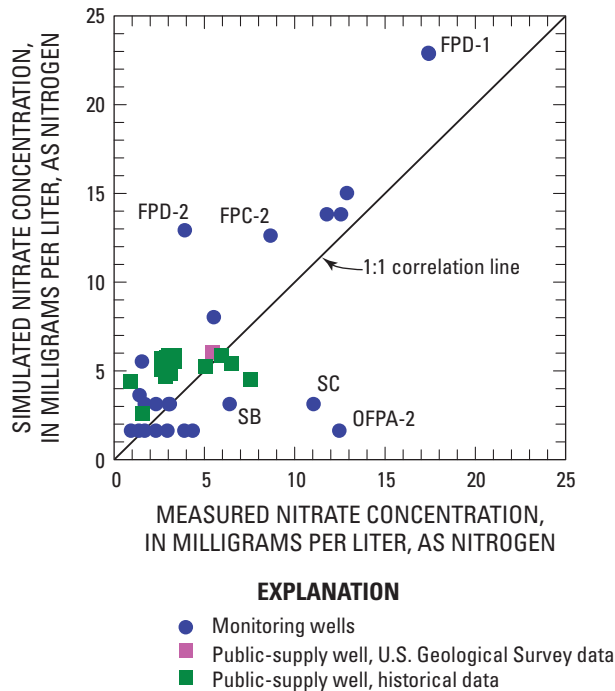


**Figure 18.** Simulated and measured concentrations of nitrate in monitoring wells and the public-supply well near Modesto, eastern San Joaquin Valley, California. Historical data from city of Modesto, written commun., 2003.

Uranium concentrations were strongly correlated ( $p < 0.01$ ,  $\rho = 0.95$ ; Spearman's rank correlation) to alkalinity (as  $\text{CaCO}_3$ ) (fig. 19). Because more alkalinity data was available than uranium data and because uranium concentrations are correlated to alkalinity, our analysis focused on alkalinity rather than uranium, and uranium concentrations in the public-supply well were inferred from alkalinity.

Sediment cores and geochemical analysis indicated that naturally-occurring uranium adsorbed to aquifer sediments has been mobilized by oxygen-rich, high-alkalinity (dominantly bicarbonate anion) water moving downward through the flow system (Jurgens and others, in press). Alkalinity has increased in shallow ground water over time. Historic data on bicarbonate alkalinity of shallow ground water indicate that concentrations were about 110 mg/L (as  $\text{CaCO}_3$ ) in 1910 (Mendenhall and others, 1916), and the median concentration in wells screened near the water table sampled in 2003–2005 was 376 mg/L (table 8). Similar to the decrease in nitrate and uranium with depth, alkalinity remains generally high (median 309 mg/L) in the shallow depth wells and decreases significantly to a median of 146 mg/L in the intermediate depth wells and a median of 85 mg/L in the deepest wells. The cause for increased alkalinity in shallow ground water is not known, although it is hypothesized that high-alkalinity water has moved downward through the unsaturated zone to the water table and subsequently moved downward

through the ground-water flow system. High alkalinity may have developed above the water table as a result of natural evaporative processes through time. After the onset of intensive irrigation and replacement of natural vegetation with crops having high transpiration rates, high-alkalinity water in the vadose zone may have moved to the water table (for example, see Lico, 1992). As ground-water pumping increased in the 1940s and 1950s, this high-alkalinity water began moving downward through the ground-water flow system, mobilizing adsorbed uranium along the way. The concept that high-alkalinity water was recharged and moved downward as agricultural development intensified is supported by statistically significant correlations between uranium and nitrate concentrations and alkalinity and nitrate concentrations ( $p = 0.013$ ,  $\rho = 0.52$  and  $p = 0.03$ ,  $\rho = 0.46$ , respectively; Spearman's rank correlation). As noted previously, nitrate concentrations increased in recharge during this time and, like high-alkalinity water, moved downward through the flow system.

Results of the particle pathline analysis were used to develop an input concentration history for alkalinity. Using the same approach as that used for the  $\text{SF}_6$ ,  $^3\text{H}$ , and nitrate comparisons, concentrations were assigned to particles on the basis of flow-weighted particle age and assuming an input concentration history based on the conceptual model described above. The input function developed that is consistent with measured concentrations assumes that alkalinity concentration before 1900 was 80 mg/L; this assumption was based on measured background concentrations in the deep monitoring wells. From 1900 to 1945, alkalinity was assumed to be 110 mg/L, an assumption based on historic concentrations before intensive agricultural development (Mendenhall and others, 1916). From 1945 to 2005, alkalinity was assumed to increase linearly with time from 110 mg/L to current concentrations of about 450 mg/L at the water table. Alkalinity of about 450 mg/L correlates to a uranium concentration of about 30  $\mu\text{g/L}$ , which is the current MCL for drinking water. This input function assumes no carbonate reactions.

Simulated alkalinity concentrations were significantly correlated to measured concentrations in the public-supply well and monitoring wells ( $p < 0.001$ ;  $\rho = 0.83$ ; Spearman's rank correlation) (fig. 20). The simulated alkalinity in the public-supply well (197 mg/L) was higher than the measured concentration (174 mg/L). Measured concentrations were lower than simulated for FPD-2 and measured concentrations were higher for OFPA-2. These differences between measured and simulated concentrations were also noted for simulated and measured nitrate and for simulated and measured tritium concentrations, further suggesting that the simulated age distributions for these wells may not adequately reflect the actual age distribution. Measured concentrations lower than simulated concentrations for wells FPD-1 and FPE-1 is consistent with dilution by low-alkalinity recharge water (Jurgens and others, in press).

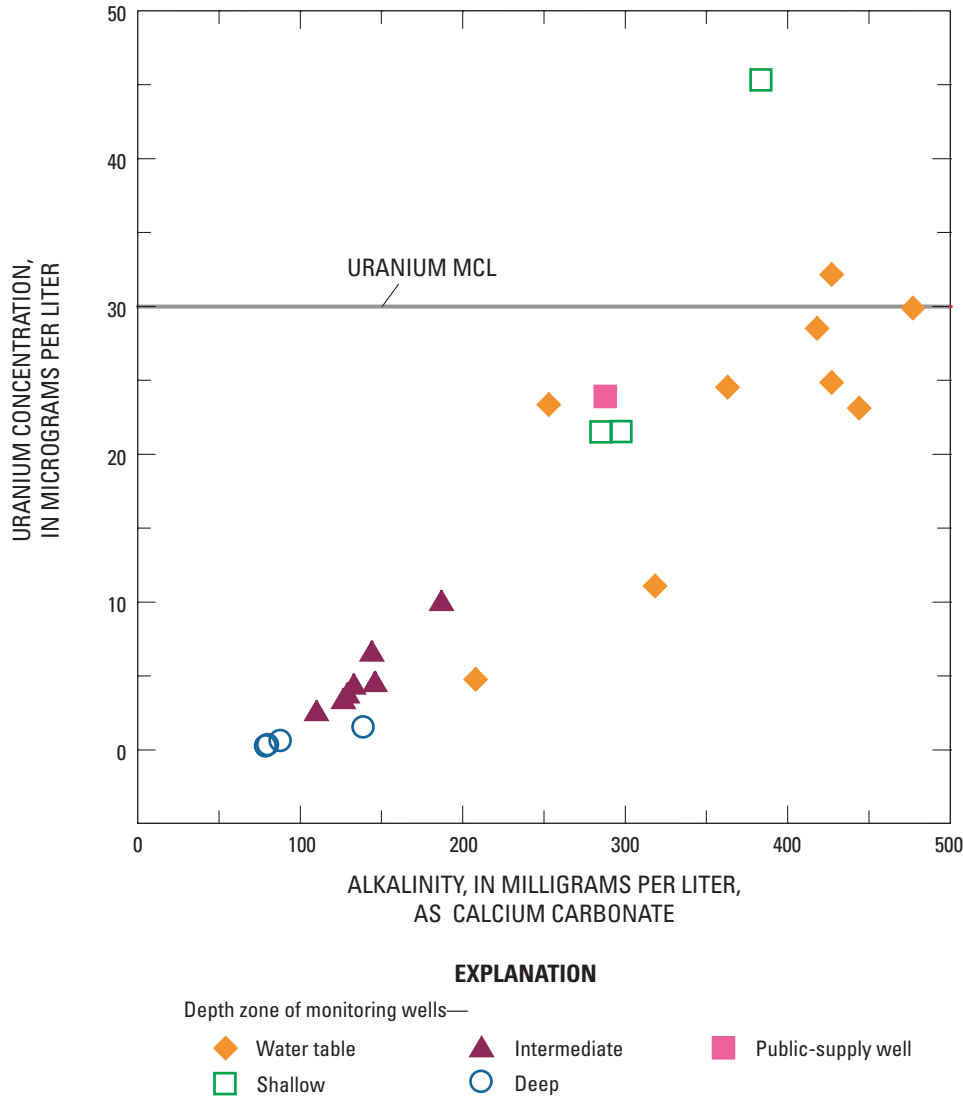


**Figure 19.** Alkalinity and uranium concentrations in monitoring wells at different depths and in the public-supply well near Modesto, eastern San Joaquin Valley, California. Depth zones for monitoring wells listed in [table 8](#). MCL, maximum contaminant level.

In summary, these results indicate that nitrate and alkalinity concentrations in recharge have increased over time. High concentrations of nitrate and alkalinity in the shallow part of the system have moved downward, and are expected to continue to move downward through the system with time. Downward movement of nitrate and alkalinity through the aquifer will continue to affect concentrations of nitrate and uranium in the public-supply well as an increasing proportion of young, affected water is contributed to the well.

### Long-Term Concentrations of Nitrate and Uranium in the Public-Supply Well

The vulnerability of the public-supply well to nonpoint source inputs of nitrate and high-alkalinity water causing

elevated concentrations of uranium is evident from the water chemistry data (Jurgens and others, in press) and the modeling analysis presented in this report. Assuming the present ground-water flow conditions persist, long-term concentrations of nitrate and uranium in the public-supply well will depend on the concentrations of nitrate and uranium at the water table in the future. Continued downward movement of ground water that is high in both nitrate and uranium will increase concentrations in the public-supply well as the proportion of younger water contributed to the well increases over time. To evaluate potential long-term nitrate and uranium concentrations in the public-supply well during the next 100 years, additional particle pathline analysis was done.

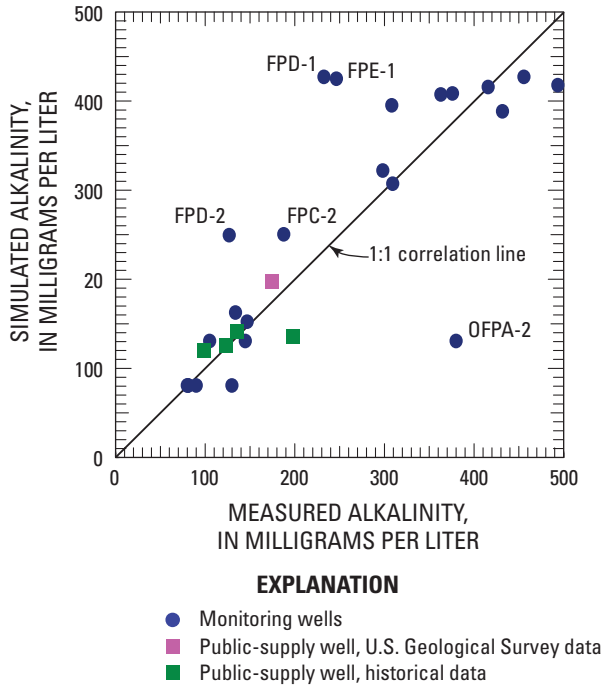


**Figure 20.** Simulated and measured alkalinity in monitoring wells and the public-supply well near Modesto, eastern San Joaquin Valley, California.

Historical data from city of Modesto, written commun., 2003.

Long-term nitrate concentrations in the public-supply well will depend on the proportion of urban and agricultural land within the contributing recharge area of the well and the amount of nitrogen input within each of these settings. Assuming the proportion of agricultural and urban land use remains fixed at the current proportion of about 70 percent urban land and 30 percent agricultural land, and assuming that the nitrate input concentrations beneath these settings remain the same (3.1 mg/L in the agricultural area and 17 mg/L in the agricultural area), simulated long-term nitrate concentrations in the public-supply well indicate that concentrations have peaked, and will decrease slightly to near 5 mg/L over the next century (fig. 21). Concentrations in the public-supply well would remain below input concentrations for at least 100 years because of the long time needed to travel to the deepest part of the public-supply well. If application rates of nitrogen fertilizer in the agricultural area increase significantly, nitrate concentrations in the public-supply well will increase. However, given the current population growth and expansion of the urban area, it is likely that this well will eventually capture water recharged entirely within the urban area. In this case, if nitrate concentrations in recharge beneath the urban area remain low, concentrations will likely continue to decrease to near 3 mg/L over the long term.

The simulated long-term nitrate concentrations in the public-supply well reflect a difference of 20 to 30 years between peak concentrations in recharge and peak concentrations in the well. This apparent time lag is the

result of the wide range of ages of water reaching the public-supply well (as a function of the distance to the well and ground-water velocity) combined with the characteristics of the input concentrations over time. An understanding of the length of time between changes in input concentrations and resulting concentrations in the public-supply well is needed to predict the impact of changes in land-use management.

Uranium concentrations do not depend on the proportion of urban and agricultural land within the CRA area because alkalinity (and uranium) concentrations are high beneath both types of land. Continued downward migration of oxygenated, high-alkalinity ground water is expected to mobilize uranium adsorbed on deeper sediments (Jurgens and others, in press). Assuming that the alkalinity near the water table remains the same (450 mg/L), simulated long-term alkalinity in the public-supply well indicates that alkalinity and uranium concentrations will increase gradually over the next 100 to 200 years (fig. 22). Simulated alkalinity flattened out at about 400 mg/L, which generally corresponds to uranium concentrations between 25 and 30  $\mu\text{g/L}$  (Jurgens and others, in press); exceptions were noted in 2 wells that had an alkalinity of less than 400 mg/L but had concentrations of uranium greater than the MCL. Although uranium concentrations would likely approach the MCL in the public-supply well over time, it will probably take more than 100 years because water with low uranium concentrations from deep in the aquifer will also contribute to the well. This allows time to evaluate management strategies and to alter well construction or pumping strategies to prohibit concentrations from exceeding the MCL.

To the extent that the conditions affecting the vulnerability of the public-supply well investigated in this study are typical of conditions affecting other public-supply wells in the Modesto region, these results can be useful in evaluating the vulnerability of other wells to nonpoint-source input of contaminants. High nitrate concentrations have been measured in shallow ground water beneath agricultural land throughout the eastern San Joaquin Valley (Burow and others, 1998; Burow and others, 2007). Because of the mostly downward movement of water in the study area and generally oxic geochemical conditions, nitrate in shallow ground water will probably continue moving downward without significant attenuation. Wells beneath a high proportion of agricultural land or wells installed in recently converted agricultural land are likely to have higher concentrations of nitrate than the public-supply well in this investigation. High alkalinity and uranium concentrations have been measured in shallow ground water in other parts of the eastern San Joaquin Valley. Public-supply wells screened in these areas may be similarly affected by uranium concentrations. Public-supply wells with shallow screened intervals containing mostly young water will likely have higher concentrations of both nitrate and uranium because of the lack of mixing with old water having low concentrations.

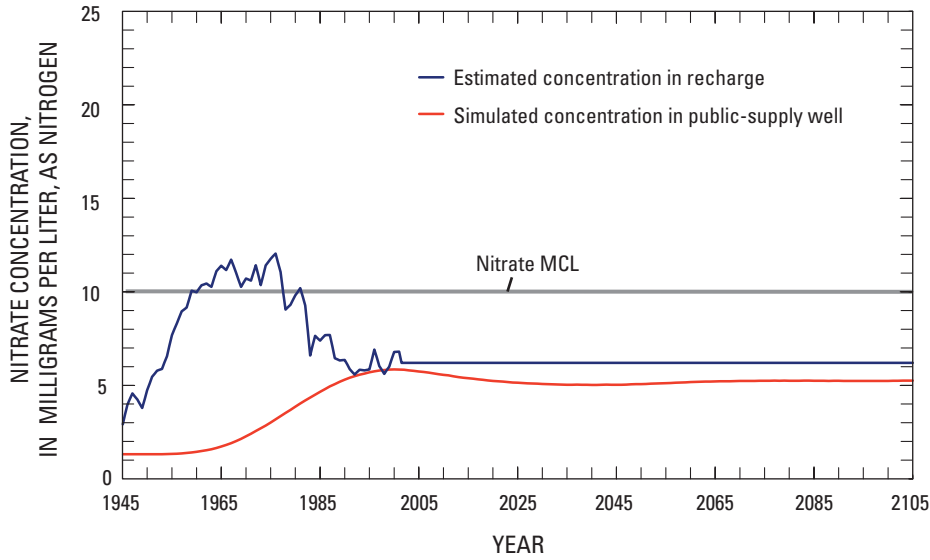


**Figure 21.** Simulated long-term concentrations of nitrate in the public-supply well near Modesto, eastern San Joaquin Valley, California. MCL, maximum contaminant level.

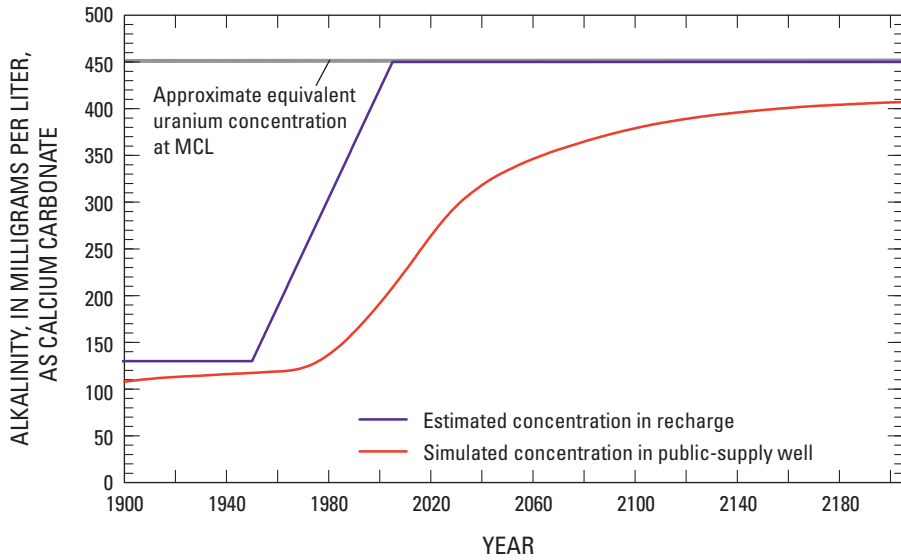


**Figure 22.** Simulated long-term alkalinity and inferred uranium concentrations in the public-supply well near Modesto, eastern San Joaquin Valley, California. MCL, maximum contaminant level.



## Model Uncertainties and Limitations

The accuracy of the ground-water flow model was limited by the assumptions used in numerical modeling to characterize the flow system; assumptions included model boundary conditions, discretization, and the effectiveness of the model calibration. The ground-water flow model was developed to portray and test the conceptual understanding of the aquifer system. The model was not expected to reproduce the natural system in detail, but to represent its dominant characteristics. Models solve for average conditions within each cell, the parameters for which are interpolated or extrapolated from measurements and estimated during calibration. Results from this model should be interpreted generally and are best suited for comparative analysis rather than for prediction at this location, although the model can predict in general terms the long-term concentrations in the public-supply well.

The accuracy of model results is related to the quality and spatial distribution of input data and of measurements used to constrain the calibration. All of the water-level data used to calibrate the local model were collected from USGS monitoring wells, which are distributed throughout the local model domain. High-quality chemical tracer data were available from a significant number of wells in the local model area to further demonstrate the ability of the model to represent overall transport through the aquifer. Stresses in the regional and local models were based on data for water year 2000, whereas detailed water levels used for calibration were for 2003–05. Longer-term water-level data indicate that climatic conditions did not change significantly between 2000 and 2005.

Estimated hydraulic conductivity values and rates of chemical transport were sensitive to the specified recharge boundary, lateral boundary conditions, and the distribution of hydrofacies. The boundary conditions for the local model relied entirely on the regional model. However, the local model area near Modesto was one of two locations in the regional model that had high-quality input data, including pumpage by well, sediment texture, and high-quality water-level measurements, so conditions in the local area were well represented in the regional model. The hydrofacies distribution was constrained by sediment texture from a significant number of wells in the local model area. The local model results were sensitive to the three-dimensional distribution of hydrofacies; however, using a similar hydrofacies approach within the domain of the same regional model, Phillips and others (2007b) determined that the estimated hydraulic conductivity values were more sensitive to changes in areal recharge and boundary fluxes than to the three-dimensional distribution of the four hydrofacies characterized in this region.

The steady-state model assumes the aquifer system is in equilibrium. Measured ground-water levels in the regional study area suggest that the ground-water system has been in a quasi-steady-state condition for many years (Phillips and others, 2007a). Prior to intensive ground-water development,

hydraulic conditions were likely much different. However, simulating post-development conditions is most appropriate to study anthropogenic influences on the quality of water in public-supply wells.

## Summary and Conclusions

A single public-supply well was selected for intensive study to evaluate the dominant processes affecting the vulnerability of public-supply wells in the Modesto area. The public-supply well, with a depth of 120 m, was selected from a set of 15 wells that represented the top 25 percent of annual pumpage in 2000. A regional ground-water flow model was used to simulate the zone of contribution (ZOC) and the contributing recharge area (CRA) for the selected well, and to choose locations for a network of 23 monitoring wells to support a detailed analysis of physical and chemical conditions and processes affecting the water chemistry in the well.

A local-scale, three-dimensional, steady-state ground-water flow and transport model was developed for this study to evaluate the age of ground-water reaching the public-supply well, and to evaluate the vulnerability of the well to nonpoint source input of nitrate and uranium. The local model is nested within the steady-state regional model that was calibrated for water year 2000. The active domain of the local model was determined by the CRA and ZOC of the public-supply well simulated using the regional-scale model.

Stresses used in the regional model were used in the local model, including discharge from ground-water pumping, and recharge from agricultural return flow, precipitation, landscape irrigation, and leakage from water distribution lines. Recharge and agricultural pumpage were determined in a water-budget analysis. The local model included both agricultural and urban land uses. Lateral boundary conditions in the local model were specified flux from the regional-scale model along approximate flow lines on the north and south boundaries and specified head from the regional-scale model on the upgradient and downgradient lateral boundaries.

The hydraulic conductivity distribution used in the local model was developed using a transition-probability-based geostatistical approach. For this study, sediments were classified into four hydrofacies categories: gravel, sand, muddy sand, and mud. Separate realizations of the hydrofacies distributions were generated for each alluvial fan aggradation sequence to reflect the unconformities produced by extensive periods of non-deposition or erosion. The resulting realizations were combined to represent the three-dimensional hydrofacies distribution for use in the local ground-water flow model. Eleven realizations were generated for each set of sequences. The model was calibrated using parameter estimation and systematic manual calibration techniques. Model results were compared to measured water levels and concentrations of age-dating tracers.

Particle tracking was used to compute pathlines and advective travel times for solutes in the local ground-water flow model, which was used to compute a refined contributing recharge area (CRA) for the public-supply well. The CRA covers about 45 km<sup>2</sup>, extending from about 0.5 km to the south and southwest of the well to about 2 km to the north and northwest of the well; it overlies both the urban and the agricultural areas. The simulated ages of particles reaching the public-supply well ranged from 9 to 30,000 years with a median of 54 years. Particle ages were weighted according to the flow associated with each particle for each layer along the well screen. The age of the ground water contributed to the public-supply well generally increased logarithmically with depth below the water table. At depths less than about 45 m below the water table, particle ages were less than 100 years. At depths more than 60 m below the water table, the particle ages ranged from 140 to 1,300 years; water in this age range was 25 percent of the flow to the well.

Most of the CRA for the public-supply well lies beneath the land area that is currently urban. Ground water within the ZOC older than about 40 years probably contains primarily agricultural-related contaminants, whereas ground water younger than 40 years probably contains both urban and agricultural contaminants because urban development began in the 1960s. Elevated concentrations of nitrate, and low concentrations of VOCs and pesticides, were measured in the public-supply well, which is consistent with concentrations in both agricultural and urban sources.

Nitrate concentrations in the ZOC of the public-supply well were highest in shallow, agriculturally-impacted ground water. The median nitrate concentration in wells screened near the water table beneath the agricultural area was 15 mg/L, whereas the median concentration in wells screened near the water table beneath the urban area was 3.1 mg/L. Nitrate concentrations decreased with depth to background concentrations of about 2 mg/L or less in the deepest monitoring wells. Nitrate concentration in the public-supply well (5.5 mg/L) was between concentrations in the shallow and the deep part of the ZOC because of the mixture of zones contributing ground water to the well. Because of the downward movement of ground water and generally oxic geochemical conditions, nitrate will move downward through the system without significant attenuation. Estimated nitrate concentrations in recharge over time, represented by measured nitrate concentrations and corresponding ground-water age-dates, indicate increasing concentrations of nitrate in recharge over time in the agricultural area. Assuming the proportion of agricultural and urban land use in the CRA of the public-supply well remains fixed at current proportions, however, and assuming that the current input concentrations beneath these settings remain the same, simulated long-term nitrate concentrations in the public-supply well indicate that concentrations have peaked, and will decrease slightly to near 5 mg/L during the next 100 years.

The simulated long-term nitrate concentrations in the public-supply well also indicate a 20- to 30-year time lag

between peak input concentrations and peak concentrations in the well. An understanding of the length of time between changes in input concentrations and resulting concentrations in the public-supply well is needed to predict the impact of changes in land-use management.

Uranium concentrations in the ZOC of the public-supply well were also highest in shallow ground water (median of 25 µg/L) and decreased with depth to background levels of about 0.5 µg/L. Sediment cores and geochemical analysis indicated that naturally-occurring uranium adsorbed to aquifer sediments is mobilized by oxygen-rich, high-alkalinity water moving downward through the flow system. Increased alkalinity at the water table in response to agricultural development resulted in increased uranium concentrations near the water table. As ground-water pumping increased in the 1940s and 1950s, this high-alkalinity water began moving downward through the ground-water flow system, mobilizing uranium along the way. On the basis of the modeling analysis, high-alkalinity, high-uranium water will likely continue to move deeper in the system. Because alkalinity (and uranium) concentrations are high beneath both the urban and agricultural land, long term uranium concentrations in the public-supply well are expected to increase as the proportion of uranium-affected water contributed to the well increases. Assuming that the alkalinity near the water table remains the same in the future, simulated long-term alkalinity in the public-supply well indicates that concentrations of uranium will increase gradually over the next 100 to 200 years. Uranium concentrations in the public-supply well will likely approach the MCL; however, it will take more than 100 years because of the old water at depth contributed to the public-supply well.

## Acknowledgments

The authors thank Lanora Hill at the city of Modesto for her consistent support and her knowledge of ground-water quality in the study area. Assistance and cooperation critical to the completion of this study were provided by numerous staff at the city of Modesto, including Jeremy Damas, William Wong, and Garner Reynolds. Thanks to Walt Ward, Joe Lima, and Mike Niemi at Modesto Irrigation District for assisting with land access and support in the installation of monitoring wells. Gary Weissmann at the University of New Mexico helped interpret core and cuttings samples, and helped develop a conceptual model of the sedimentary sequences in the subsurface. Graham Fogg at the University of California at Davis helped develop the spatial correlation model of aquifer hydrofacies and provided input on parts of the model calibration and sensitivity analysis. Sandy Eberts provided critical support and facilitated a transfer of knowledge among the TANC team and other scientists in the USGS.

## References Cited

- Alexander, R.B., and Smith, R.A., 1990, County level estimates of nitrogen and phosphorus fertilizer use in the United States, 1945 to 1985: U.S. Geological Survey Open-File Report 90-130, 12 p.
- Barlow, P.M., 1997, Particle-tracking analysis of contributing areas of public-supply wells in simple and complex flow systems, Cape Cod, Massachusetts: U.S. Geological Survey Water-Supply Paper 2434, 66 p.
- Bartow, J.A., 1991, The Cenozoic evolution of the San Joaquin Valley, California: U.S. Geological Survey Professional Paper 1501, 40 p.
- Böhlke, J.K., 2002, Groundwater recharge and agricultural contamination: *Hydrogeology Journal*, v. 10, no. 1, p. 153–179.
- Böhlke, J.K., 2005, Tracermodell1. Excel workbook for calculation and presentation of environmental tracer data for simple groundwater mixtures, *in* International Atomic Energy Agency guidebook on the use of chlorofluorocarbons in hydrology: Vienna, International Atomic Energy Agency, p. 202–206.
- Böhlke, J.K., and Denver, J.M., 1995, Combined use of groundwater dating, chemical, and isotopic analyses to resolve the history and fate of nitrate contamination in two agricultural watersheds, Atlantic coastal plain, Maryland: *Water Resources Research*, v. 31, no. 9, p. 2319–2339.
- Bouwer, Herman, 1978, *Groundwater hydrology*: New York, McGraw-Hill Book Company, 480 p.
- Brown, C.J., Colabufo, S., and Coates, J.D., 2002, Aquifer geochemistry and effects of pumping on ground-water quality at the Green Belt Parkway Well Field, Holbrook, Long Island, New York: U.S. Geological Survey Water-Resources Investigations Report 01-4025, 21 p.
- Burow, K.R., Dubrovsky, N.M., and Shelton, J.L., 2007, Temporal trends in concentrations of DBCP and nitrate in groundwater in the eastern San Joaquin Valley, California, USA: *Hydrogeology Journal*, v. 15, no. 5, p. 991–1007.
- Burow, K.R., Shelton, J.L., and Dubrovsky, N.M., 1998, Occurrence of nitrate and pesticides in ground water beneath three agricultural land-use settings in the eastern San Joaquin Valley, California, 1993–1995: U.S. Geological Survey Water-Resources Investigations Report 97-4284, 51 p.
- Burow, K.R., Shelton, J.L., and Dubrovsky, N.M., in press, Nitrate and pesticide trends in ground water in the eastern San Joaquin Valley, California: *Journal of Environmental Quality*, approved July 24, 2007.
- Burow, K.R., Shelton, J.L., Hevesi, J.A., and Weissmann, G.S., 2004, Hydrogeologic characterization of the Modesto area, San Joaquin Valley, California: U.S. Geological Survey Scientific Investigations Report 2004-5232, 54 p.
- Burow, K.R., Weissmann, G.S., Miller, R.D., and Placzek, Gary, 1997, Hydrogeologic facies characterization of an alluvial fan near Fresno, California, using geophysical techniques: U.S. Geological Survey Open-File Report 97-46, 15 p.
- Busenberg, E., and Plummer L.N., 2000, Dating young ground water with sulfur hexafluoride: Natural and anthropogenic sources of sulfur hexafluoride: *Water Resources Research*, v. 36, p. 3011–3030.
- California Department of Finance, 2006, California county population estimates and components of change by year, July 1, 2000–2006: Sacramento, California, December 2006, accessed August 10, 2007 at [http://www.dof.ca.gov/HTML/DEMOGRAP/ReportsPapers/Estimates/E2/E-2\\_2000-06.asp](http://www.dof.ca.gov/HTML/DEMOGRAP/ReportsPapers/Estimates/E2/E-2_2000-06.asp)
- Carle, S.F., 1997, Implementation schemes for avoiding artifact discontinuities in simulated annealing: *Mathematical Geology*, v. 29, no. 2, p. 231–244.
- Carle, S.F., 1999, T-PROGS: transition probability geostatistical software: User's Manual: Davis, Calif., University of California, 76 p.
- Carle, S.F., and Fogg, G.E., 1996, Transition probability-based indicator geostatistics: *Mathematical Geology*, v. 28, no. 4, p. 453–476.
- Carle, S.F., and Fogg, G.E., 1997, Modeling spatial variability with one- and multi-dimensional continuous-lag Markov chains: *Mathematical Geology*, v. 29, no. 7, p. 891–918.
- Carle, S.F., LaBolle, E.M., Weissmann, G.S., VanBrocklin, David, and Fogg, G.E., 1998, Geostatistical simulation of hydrostratigraphic architecture, a transition probability/Markov approach, *in* Concepts in Hydrogeology and Environmental Geology: SEPM (Society for Sedimentary Geology), Special Publication no. 1, p. 147–170.
- Cook P.G., and Böhlke, J.K., 1999, Determining timescales for groundwater flow and solute transport, *in* Cook, Peter, and Herczeg, A.L., *Environmental Tracers in Subsurface Hydrology*: Boston, Kluwer Academic Publishers, p. 1–30.
- Cole, B.E., and Silliman, S.E., 2000, Utility of simple models for capture zone delineation in heterogeneous unconfined aquifers: *Ground Water*, v. 38, no. 5, p. 665–672.
- Dalgish, B.A., 2006, Hydrogeologic characterization and groundwater flow model analyses in Modesto, California: University of California Davis, unpublished Master's thesis, May 2006, 106 p.



- Davis, S.N., and Hall, F.R., 1959, Water-quality of eastern Stanislaus and northern Merced counties, California: Stanford, Calif., Stanford University Publications, Geological Sciences, v. 6, no. 1, 112 p.
- Domenico, P.A., and Schwartz, F.W., 1998, Physical and chemical hydrogeology, 2d ed.: New York, John Wiley and Sons, 506 p.
- Dubrovsky, N.M., Kratzer, C.R., Brown, L.R., Gronberg, J.M., and Burow, K.R., 1998, Water quality in the San Joaquin–Tulare Basins, California, 1992–95: U.S. Geological Survey Circular 1159, 38 p.
- Eberts, S.M., Erwin, M.L., and Pixie, A.H., 2005, Assessing the vulnerability of public-supply wells to contamination from urban, agricultural, and natural sources: U.S. Geological Survey Fact Sheet 2005-3022, 4 p.
- Focazio, M.J., Reilly, T.E., Rupert, M.G., and Helsel, D.R., 2002, Assessing ground-water vulnerability to contamination—Providing scientifically defensible information for decision makers: U.S. Geological Survey Circular 1224, 33 p.
- Fleckenstein, J.H., Niswonger, R.G., and Fogg, G.E., 2006, River-aquifer interactions, geologic heterogeneity, and low-flow management: *Ground Water*, v. 44, no. 6, p. 837–852.
- Franke, O.L., Reilly, T.E., Pollock, D.W., and LaBaugh, J.W., 1998, Estimating areas contributing recharge to wells—Lessons from previous studies: U.S. Geological Survey Circular 1174, 14 p.
- Freeze, R.A., and Cherry, J.A., 1979, *Groundwater*: Englewood Cliffs, N.J., Prentice-Hall, 604 p.
- Gilliom, R.J., Barbash, J.E., Crawford, C.G., Hamilton, P.A., Martin, J.D., Nakagaki, N., Nowell, L.H., Scott, J.C., Stackelberg, P.E., Thelin, G.P., and Wolock, D.M., 2006, Pesticides in the nation’s streams and ground water, 1992–2001: U.S. Geological Survey Circular 1291, 172 p.
- Gronberg, J.M., Dubrovsky, N.M., Kratzer, C.R., Domagalski, J.L., Brown, L.R., and Burow, K.R., 1998, Environmental setting and study design for assessing water quality in the San Joaquin-Tulare basins, California: U.S. Geological Survey Water-Resources Investigations Report 97-4205, 45 p.
- Halford, K.J. and Hanson, R.T., 2002, User guide for the drawdown-limited, Multi-Node Well (MNW) Package for the U.S. Geological Survey’s Modular Three-Dimensional Finite-Difference Ground-Water Flow Model, Versions MODFLOW-96 and MODFLOW-2000: U.S. Geological Survey Open-File Report 02-293, 33 p.
- Harbaugh, A.W., Banta, E.R., Hill, M.C., and McDonald, M.G., 2000, MODFLOW-2000, the U.S. Geological Survey modular ground-water model—User guide to modularization concepts and the ground-water flow process: U.S. Geological Survey Open-File Report 00-92, 121 p.
- Harrar, W. G., Sonnenborg, T. O., and Henriksen, H. J., 2003, Capture zone, travel time and solute transport predictions using inverse modelling and different geological models: *Hydrogeology Journal*, v. 11, no. 5, p. 536–548.
- Hill, M.C., Banta, E.R., Harbaugh, A.W., and Anderman, E.R., 2000, MODFLOW-2000, the US Geological Survey Modular Ground-Water Model—User guide to the observation, sensitivity, and parameter-estimation processes and three post-processing programs: U.S. Geological Survey Open-File Report 00-184, 209 p.
- Hutson, S.S., Barber, N.L., Kenny, J.F., Linsey, K.S., Lumia, D.S., and Maupin, M.A., 2004, Estimated use of water in the United States in 2000: U.S. Geological Survey Circular 1268, 52 p.
- Johnson, R., Pankow, J.F., Bender, D.A., Price, C.V., and Zogorski, J.S., 2000, MTBE—To what extent will past releases contaminate community water supply wells?: *Environmental Science & Technology*, v. 34, no. 9, p. 210A–217A.
- Jurgens, B.C., Burow, K.R., Dalgish, B.A., and Shelton, J.L., in press, Hydrogeology, water chemistry, and factors affecting the transport of contaminants in eastern San Joaquin, Valley, California: U.S. Geological Survey Scientific Investigations Report 2008-5156.
- Kauffman, L.J., Baehr, A.L., Ayers, M.A., and Stackelberg, P.E., 2001, Effects of land use and travel time on the distribution of nitrate in the Kirkwood-Cohansey aquifer system in southern New Jersey: U.S. Geological Survey Water-Resources Investigations Report 01-4117, 49 p.
- Lico, M.S., 1992, Detailed study of irrigation drainage in and near wildlife management areas, west-central Nevada, 1987–90; part A. Water quality, sediment composition, and hydrogeochemical processes in Stillwater and Fernley wildlife management areas: U.S. Geological Survey Water-Resources Investigations Report 92-4024A, 65 p.
- Londquist, C.J., 1981, Digital model of the unconsolidated aquifer system in the Modesto area, Stanislaus and San Joaquin Counties, California: U.S. Geological Survey Water-Resources Investigations Report 81-12, 36 p.

- Marchand, D.E., and Allwardt, A., 1981, Late Cenozoic stratigraphic units, northeastern San Joaquin Valley, California: U.S. Geological Survey Bulletin 1470, 70 p.
- Mendenhall, W.C., Dole, R.B., and Stabler, Herman, 1916, Ground water in San Joaquin Valley, California: U.S. Geological Survey Water-Supply Paper 398, 310 p.
- Michel, R.L., 1989, Tritium deposition in the continental United States, 1953–83: U.S. Geological Survey Water-Resources Investigations Report 89-4072, 46 p.
- National Oceanic and Atmospheric Administration, 2005, Precipitation data: accessed November 14, 2005, at <http://lwf.ncdc.noaa.gov/oa/pub/data/coop-precip/california.txt>
- National Research Council, 1993, Ground-water vulnerability assessment—Predicting relative contamination potential under conditions of uncertainty: Washington, D.C., National Academy Press, 204 p.
- Nolan, B.T., and Stoner, J.D., 2000, Nutrients in ground waters of the conterminous United States, 1992–1995: Environmental Science and Technology, v. 34, no. 7, p. 1156–1165.
- Page, R.W., 1986, Geology of the fresh ground-water basin of the Central Valley, California with texture maps and sections: U.S. Geological Survey Professional Paper 1401-C, 54 p.
- Page, R.W. and Balding, G.O., 1973, Geology and quality of water in the Modesto–Merced area San Joaquin Valley, California: U.S. Geological Survey Water Resources Investigations Report 6-73, 85 p.
- Paschke, S.S., Kauffman, L.J., Eberts, S.M., Hinkle, S.R., 2007, Overview of regional studies of the transport of anthropogenic and natural contaminants to public-supply wells, *section 1*, in Paschke, S.S., ed., Hydrogeologic settings and ground-water flow simulations for regional studies of the transport of anthropogenic and natural contaminants to public-supply wells—studies begun in 2001: Reston, Va., U.S. Geological Survey Professional Paper 1737-A, p. 1-1–1-18.
- Phillips, S.P., Burow, K.R., Rewis, D.L., Shelton, J.L., and Jurgens, B.J., 2007a, Hydrogeologic settings and ground-water flow simulations of the San Joaquin Valley regional study area, California, *section 4*, in Paschke, S.S., ed., Hydrogeologic settings and ground-water flow simulations for regional studies of the transport of anthropogenic and natural contaminants to public-supply wells—studies begun in 2001: Reston, Va., U.S. Geological Survey Professional Paper 1737-A, p. 4-1–4-31.
- Phillips, S.P., Green, C.C., Burow, K.R., Shelton, J.L., and Rewis, D.L., 2007b, Development of regional- and local-scale ground-water flow models of part of the northeastern San Joaquin Valley, California: U.S. Geological Survey Scientific Investigations Report 2007–5009, 43 p.
- Pollock, D.W., 1994, Source code and ancillary data files for the MODPATH particle tracking package of the ground-water flow model MODFLOW; version 3, release 1: U.S. Geological Survey Open-File Report 94-0463, 6 p., 2 diskettes.
- Reilly, T.E., and Gibs, J., 1993, Effects of physical and chemical heterogeneity of water-quality samples obtained from wells: Ground Water, v. 31, no. 5, p. 805–813.
- Reilly, T.E., and Pollock, D.W., 1993, Factors affecting areas contributing recharge to wells in shallow aquifers: U.S. Geological Survey Water-Supply Paper 2412, 21 p.
- Reilly, T. E., and Pollock, D. W., 1995, Effect of seasonal and long-term changes in stress on sources of water to wells: U.S. Geological Survey Water-Supply Paper 2445, 25 p.
- Ruddy, B.C., Lorenz, D.L., and Mueller, D.K., 2006, County-level estimates of nutrient inputs to the land surface of the conterminous United States, 1982–2001: U.S. Geological Survey Scientific Investigations Report 2006–5012, 17 p.
- Squillace, P.J., Moran, M.J., and Price, C.V., 2004, VOCs in shallow groundwater in new residential/commercial areas of the United States: Environmental Science and Technology, v. 38, no. 20, p. 5327–5338.
- U.S. Environmental Protection Agency, 2006, 2006 Edition of the drinking water standards and health advisories: U.S. Environmental Protection Agency, Office of Water, EPA-822-R-06-013, accessed December 11, 2006 at <http://www.epa.gov/waterscience/criteria/drinking/dwstandards.pdf>
- Weissmann, G.S., and Fogg, G.E., 1999, Multi-scale alluvial fan heterogeneity modeled with transition probability geostatistics in a sequence stratigraphic framework: Journal of Hydrology, v. 226, no. 1-2, p. 48–65.
- Weissmann, G.S., Mount, J.F., and Fogg, G.E., 2002, Glacially driven cycles in accumulation space and sequence stratigraphy of a stream-dominated alluvial fan, San Joaquin Valley, California, USA: Journal of Sedimentary Research, v. 72, no. 2, p. 240–251.
- Weissmann, G.S., Yong, Z., Fogg, G.E., and Mount, J.F., 2004, Influence of incised valley fill deposits on hydrogeology of a glacially-influenced, stream-dominated alluvial fan, in Bridge, J., and Hyndman, D.W., Aquifer Characterization: SEPM (Society for Sedimentary Geology) Special Publication 80, p. 15–28.

- Wilber, W.G., and Couch, C.A., 2002, Assessing five national priorities in water resources: American Water Resources Association, *Water Resources IMPACT*, v. 4, no. 4, p. 17–21.
- Wright, M.T., Belitz, Kenneth, Johnson, T., 2004, Assessing the susceptibility to contamination of two aquifer systems used for public water supply in the Modesto and Fresno metropolitan areas, California, 2001 and 2002: U.S. Geological Survey Scientific Investigations Report 2004-5149, 35 p.
- Zogorski, J.S., Carter, J.M., Ivahnenko, Tamara, Lapham, W.W., Moran, M.J., Rowe, B.L., Squillace, P.J., and Toccalino, P.L., 2006, The quality of our Nation's waters—volatile organic compounds in the Nation's ground water and drinking-water supply wells: U.S. Geological Survey Circular 1292, 101 p.

